Integration of diagenesis in basin-scale, stratigraphic forward models using reactive transport modeling: input and scaling issues.

HAMON Youri [(1)], BACHAUD Pierre [(1)], GRANJEON Didier [(1)], BEMER Elisabeth [(1)], CARVALHO Ancilla Maria Almeida [(1, 2)]

(1) IFPEN, Direction Géosciences, 1 et 4 Avenue de Bois-Préau, 92852 Rueil-Malmaison Cedex. France

(2) PETROBRAS S. A., Av. Henrique Valadares, 28, Rio de Janeiro-RJ, 20231-030, Brazil.

*e-mail address of corresponding author: youri.hamon@ifpen.fr

Keywords: Stratigraphic forward modeling, Reactive-transport modeling, Mixed sedimentation, Early diagenesis

ABSTRACT *(The abstract should not exceed 300 words)*

This article presents an integrated approach based on stratigraphic forward modeling and reactive transport modeling to adequately represent the development of a mixed siliciclastic-carbonate sedimentary system and its diagenesis. This work was realized on a realistic case study, the Oligo-Miocene series of Carry-le-Rouet, South-East of France, characterized by a complex pattern of bioclastic, bioconstructed and siliciclastic deposits, and affected by several exposure surfaces and associated meteoric diagenesis. A first phase consisted in building a stratigraphic forward model (SFM), using the software Dionisos^{Flow}. The construction of the model was based on sensitivity tests on the two main parameters controlling basin sedimentation: 1) competition between carbonate production and siliciclastic supply; 2) subsidence. The results of the simulations, especially the facies distribution, the thickness of the deposits and the sedimentary architectures were compared with the observed data to validate the model. A second phase consisted in focusing on a specific stratigraphic event and performing reactive transport modeling (RTM) on a 2D section extracted from the Dionisos^{Flow} model to evaluate the mineralogical transformations and resulting petrophysical evolutions created by early diagenesis. The calculation results show the occurrence of two domains of salinity, that were associated with two distinct diagenetic environments: marine and meteoric phreatic. Globally, the simulated diagenetic trends are qualitatively consistent with the petrographic observations, except for the replacement of aragonite by a calcite cement, that systematically occurred in the model and is not always observed in thin sections. This preliminary study emphasizes the issues associated with the application of RTM to diagenetic phenomena, linked with the uncertainties inherent to specific parameters, such as minerals kinetic properties, and the mismatch between the space and time scales of the modeled processes and the upscaled description of each SFM cell. These results argue in favor of an alternative solution, that could conciliate the different processes. The combination of the various SFM output properties with simplified chemical reactions whose rates have been tuned for specific diagenetic processes of interest could provide diagenetic risk maps that would constitute useful guides for exploration at basin scale.

1. INTRODUCTION

Exploration of carbonate prospects in remote basins is classically considered complex, with geological heterogeneities coming in several types (stratigraphic architecture, facies distribution and heterogeneity, diagenetic overprint) and at several scales (field scale, well scale, microscale), sparse data in subsurface, and difficulties of seismic interpretation due to their large variability of acoustic properties (Yose et al., 2006). Numerical modeling can be used to tackle such challenges and to mitigate risk, but one of the fundamental conceptual and technical challenge is to be able to consider the impact of diagenesis in such models (Nader, 2017). There is a wealth of published work about this topic, depicting different approaches according to the scale and purpose of the study:

Carbonate sedimentary facies and their related diagenetic heterogeneities can be modeled using geostatistical approaches. A wide range of methods and algorithms have been developed in the past (Lantuéjoul, 2001), up to advanced geostatistical techniques, such as nested, plurigaussian and bi-plurigaussian simulations used to reproduce diagenetic trends (Barbier, 2012; Blázquez-Fernández et al., 2013; Hamon et al., 2016; Carrera et al., 2018). However, such numerical models are based on geostatistics and only give multiple equiprobable representations of the reservoir, without considering the specificities of each diagenetic process. Moreover, they require a quantification of the diagenetic products (i.e. petrographic estimations, well-log interpretation) often rendered difficult by the scarcity and the poor representativity of the data (Nader, 2017; De Boever et al., 2018). Thus, the resulting images can be unrealistic and unreliable in predictions.

Reactive transport modeling (RTM) has been widely used as it is a powerful tool to evaluate mineralogical and petrophysical transformations induced by fluid-rock interactions in geological phenomena (Steefel et MacQuarrie, 1996). Its use in 1D or simplified 2D models mainly aims to validate conceptual diagenetic models or discuss the influence of the factors involved in a diagenetic process. Thus, dolomitization processes has been extensively modeled (Whitaker et al., 2004):

geothermal convection (Caspard et al., 2004; Whitaker and Xiao, 2010), hydrothermal dolomitization (Salas et al., 2007; Blomme et al., 2017), burial compaction-driven dolomitization (Consonni et al. 2010), early evaporative and reflux dolomitization (Al-Helal et al, 2012; Gabellone and Whitaker 2015; Lu and Cantrell, 2016; Yapparova et al., 2017), and even dedolomitization (Ayora et al., 1998). Far less has been published concerning meteoric or mixing zone diagenesis (Rezaei et al., 2005; Xiao and Jones, 2006; Cooper et al., 2014; Zhao et al., 2017). Moreover, given the usual 1D or 2D aspect of this approach, these models generally do not consider the sedimentary background (i.e. environments and processes), or the common impact of extrinsic factors (i.e. spatial distribution of fluids, temperatures). Finally, those models are generally outcrop- or well-scale models and are therefore limited in size (Gabbelone et al., 2016).

A few papers developed a dual approach, with numerical forward modeling of carbonate sedimentology and diagenesis, mainly in two dimensions (Matthews and Frohlich, 1987; CARB3D+ of Whitaker et al., 1999; Paterson et al., 2008, Berra et al., 2016; Facies-3D of Matsuda et al., 2004). The main drawback of these approaches is that they require some major assumptions on input parameters when performed on fossil case studies (i.e. original mineralogy, depositional petrophysical properties, fluid chemical compositions, diagenesis rates). These parameters can be derived from outcrop analog studies (Berra et al., 2016) or from uniformitarian hypotheses (using present-day values) but remain unsure. New types of rule-based models, such as cellular automata, have also been developed to represent the interaction of many different elements of carbonate deposition and diagenesis. The idea here is to mimic fluid flow and diagenetic effect without an explicit model of the flow and the physico-chemical reactions (Planteblat et al., 2012; Planteblat, 2013; Lanteaume et al., 2018).

Finally, the combination of stratigraphic forward modeling (SFM) and reactive transport modeling (RTM) to jointly represent the development of a carbonate sedimentary system and its early diagenesis has been rarely done (Nader, 2017). This article presents the results of an integrated

study, based on a geological characterization and modeling of a well-constrained, real (not generic) case study, namely the Oligo-Miocene series of Carry-le-Rouet, South-East of France. The SFM is used to obtain a realistic sedimentological framework at a given time step, at which, RTM is used to simulate the effect of meteoric diagenesis associated to exposure. This methodological study aims at evaluating how RTM could be added to a SFM workflow to assess the impact of early diagenesis processes on mineralogy and petrophysical properties, at basin scale. Specifically, we aim to shed light on the constraining data that can be used at large-scale and the way they can be derived from outcrop data, as well as uniformitarian constraints from modern analogues. Finally, the scale compatibility between both approaches (SFM and RTM) is discussed to define the limits and the type of results we can expect from such an approach.

2. METHODS

2.1. Stratigraphic forward modeling

SFM is designed to integrate data with different scales and resolutions and is used to provide a better understanding of the sedimentary processes and resulting architectures (quantitative point of view) where data are scarce. The modeling software used in this study is Dionisos^{Flow}, a 3D process-based stratigraphic forward model (Granjeon, 1997), which simulates the long-term (100 ky to 100 My) and large-scale (10 to 100 km) evolution of sedimentary basins. Dionisos^{Flow} can reproduce both siliciclastic and carbonate deposits, the concentration of sediments in each cell depending on the erosion, production, transport, and depositional processes. Several authors have presented their works with Dionisos^{Flow} in lacustrine systems (Yin et al., 2015; Csato et al., 2015), deltaic systems (Burgess et al., 2006), marine carbonate systems (William et al., 2011; Seard et al., 2013), mixed siliciclastic-carbonate systems (Kolodka et al., 2016) and turbidite systems (Deville et al., 2015).

A forward stratigraphic simulation is performed from an initial sedimentary topography within a specific time interval subdivided in a set of time steps. At each time step, three main physical processes are simulated (Granjeon and Joseph, 1999; Granjeon, 2014): (1) the creation or removal of accommodation space controlled by eustasy and tectonics, defined through the input of a user-defined sea-level curve and subsidence maps generated from geological or seismic information; (2) the sediment supply located at the model boundaries and the in situ carbonate production, which could be simulated as a function of age, water depth, and environmental conditions such as waves and drift energies (e.g. Seard et al., 2013; Liechoscki de Paula Faria et al., 2017); (3) the transport of sediments, modeled by the diffusion equation that determines the sediment flux from the water flow (rivers, streams) and slope.

2.2. Reactive transport modeling

Reactive transport simulations were performed using Coores-Arxim software, that couples a geochemical calculation code (Arxim-LMA, for Law of Mass Action; Moutte, 2009) with the multicomponent, multiphase, non-isothermal reservoir simulator Coores through a sequential splitting strategy solving successively the multiphase flow and the reactive transport (Trenty et al., 2006). In this method, the Law of Mass Action approach (LMA) calculates the solution speciation under the constraints of mass conservation and chemical equilibrium between aqueous species. Fluid-rock interactions are accounted for through kinetic reactions depending, among other parameters, on the distance to equilibrium, mineral reactive surface area and catalytic or inhibiting effect of specific aqueous species (Lasaga, 1984). Coores-Arxim software has been applied to study various geosciences problems, such as CO_2 geological storage (Estublier et al., 2013), dolomitization (Blomme et al., 2017) or hydrogen genesis in ophiolites (Bachaud et al., 2017).

3. THE CARRY-LE-ROUET CASE STUDY

This modeling work is based on the Oligo-Miocene succession, outcropping in the region of Carry-le-Rouet (South-East of France). This succession is characterized by a complex pattern of bioclastic, bioconstructed and siliciclastic deposits, organized in numerous depositional cycles of mixed carbonate–siliciclastics (Oudet et al., 2010). Moreover, recent studies have highlighted the importance of several sedimentary discontinuities, considered as exposure surfaces, and potentially associated to early meteoric diagenesis (Santerre, 2010; Hamon et al., 2013).

3.1. Geodynamic and structural setting

The Oligo-Miocene series outcropping in the Carry-le-Rouet – Sausset-les-Pins region had been deposited unconformably on the early Cretaceous limestones of the Nerthe Massif, a Pyrenean E–W trending thrust structure (Fig. 1A). The Nerthe area also corresponds to the northern margin of the Liguro-Provençal Basin (Fournier et al., 2016). The latter is localized in the northwestern part of the Mediterranean Sea. Its northern and southern margins correspond to the modern Golfe du Lyon and West Sardinia, respectively. The Liguro-Provençal Basin opened during Late Oligocene and Aquitanian stages, by anticlockwise rotation and southeastward drift of the Corsica-Sardinia continental block (Séranne et al., 1995; Gattacceca et al., 2007). This basin is a half-graben characterized by a rollover process and a syn-tectonic diverging basin-fill, indicating the control by an extensional listric fault. During the rifting period, pre-existing NW-SE structures are preferentially reactivated by extension which might have an impact on the stratigraphy. Indeed, the discontinuities SB0, SB2 and SB3 (Fig. 1C) correspond to low-angle (1° to 9°) angular unconformities (Oudet et al., 2010). Moreover, during this rifting period, most of the Golfe du Lyon is exposed and suffered an important subaerial erosion potentially providing a high siliciclastic sediment flux and explaining the mixed sedimentation (Bache, 2008).

3.2. Stratigraphy and sedimentary conceptual model

The Carry-le-Rouet Oligo-Miocene succession (Fig. 1C) has been the object of numerous studies, as it is one of the only onshore, continuous series of the northern margin of the Liguro-Provençal Basin. Facies, depositional environments and associated paleogeography have been extensively examined by many authors, who described more than twenty different facies (Andreieff et al., 1972; Nury, 1990; Nury and Thomassin, 1994; Galloni, 2003; Conesa et al., 2005; Oudet et al., 2010; Demory et al., 2011; Conesa et al., 2014). In the present study, for modeling purposes, they have been summarized and grouped into a synthetic facies' classification composed of only ten facies (Table 1), used hereafter as modeling inputs. Limited additional field work was performed, to quality check the previous works and the consistency of the classification proposed in Table 1.

In order to constrain the facies spatial distribution and relationships, a 3D conceptual geological model of the Oligo-Aquitanian series in the Carry-le-Rouet area is proposed in Figure 2. This scheme illustrates the general architecture of the sedimentary system and emphasizes the mixing of carbonate and siliciclastic deposits. As proposed by Oudet (2008), the study area may be considered as the northern termination of a SW-NE elongated gulf, opened to the marine domain toward the South (Fig. 1B), in which a carbonate shelf system settled down. This system is affected by an important fluvial siliciclastic input that mixed with the background carbonate sedimentation (Oudet, 2008, Santerre, 2010). Coralgal patch reefs developed in a fringing position or as isolated patch reefs in this lagoonal setting. Barrier reefs that isolated this area from the open sea were not observed at the study outcrop but were mentioned and associated with domal morphologies on seismic interpretation (Chevalier, 1961, Oudet, 2008). The presence of conglomeratic deposits in the most proximal setting suggests that the coastline was locally bordered by littoral cliffs. This is also consistent with the observation of a low-relief escarpment (Fig. 2).

The study series have been divided into four stratigraphic units, following the sequence stratigraphic framework of Oudet et al. (2010). The first one lies on a basal unconformity, affecting the Lower Cretaceous limestones of the Nerthe Massif onshore and potential Lower Oligocene (Rupelian) continental deposits in the Bay of Marseille (e.g. Fournier et al., 2016). It corresponds to terrigenous alluvial and fluvial deposits (well stratified clays and sandstones) and freshwater palustrine limestones. Based on cored samples and structural continuity with the Rupelian continental deposits from L'Estaque area (15 km East of our study area), the first unit is dated from the Late Rupelian to Early Chattian period (Fournier et al., 2016). On our study area, this unit is only observed offshore on low resolution, old industrial seismic data (Oudet, 2008).

The second unit corresponds to the "S-Olig." sequence of Oudet et al. (2010) (Fig. 1C), who dated it from Late Chattian to Early Aquitanian (based on palynologic and magnetostratigraphic studies). The base of the unit (Conglomeratic Rouet lithologic unit) is mainly composed of channelized conglomerates (F1) and sandstones (F2), embedded in clayey siltstone matrix, interpreted as sheetfloods at the mouth of a gravely river or a small fan delta. Progressively, marine influences are present, marked by the appearance of marine bioturbation (Thalassinoides), marine fauna (Ostreidae, Serpulidae) and the onset of scattered coral colonies (bafflestones) occurring in a coral-rich rudstone (F7). The top of the S-Olig unit (Parareefal Cap de Nautes lithologic Unit) is dominated by the alternation of quartz-rich bioclastic wackestones (F4 and F5) and silty marls beds (F6), moderately to heavily bioturbated and rich in coal fragments. Facies F4 exhibits mixed faunal remains, with bioclasts of gastropods, bivalves, echinoids, Teredinidae shelly tubes, Vermetidae shells, coral debris and Serpulidae. F4 has been interpreted as deposited in a shallow inner-shelf setting with moderate-energy. Facies F5 is characterized by the presence of many benthic foraminifers (Miliolidae, Austrotrillinidae, Amphisteginidae, Lepidocyclinidae, Myogypsinidae) associated with bioclasts of bivalves, echinoids, and red algae. These deposits are interpreted as low-energy, stenohaline, inner- to mid-shelf deposits, emplaced in slightly deeper and distal conditions than F4. Finally, based on the lack of fauna, the presence of lignite clasts and the fine-grained

texture, facies F6 is interpreted as a low-energy, badly oxygenated deeper inner-shelf facies. At two different stratigraphic level of the unit (from 14 to 20 m and from 31 to 32 m; Fig. 1C), laterally discontinuous beds of facies F7 and F8 are interbedded in these lithologies. Facies F8 consists of coral and red algae framestones to bafflestones, forming flat layers of low topographic relief (maximum 2 m thick), and a few hundreds of meters of lateral extent. This facies has been interpreted as isolated frame-building coral carpets in inner-shelf setting. Facies F7 mostly consists of coral-rich rudstones, interpreted as reworking breccia, in which isolated, non-frame-building coral colonies are present (coral bafflestones). Facies F7 can covered several hundreds of meters to a few kilometers of lateral extent.

The third unit correspond to the "S-1 Aquit." sequence of Oudet et al. (2010), dated from Aquitanian (Fig. 1C). Its basal part (Brackish Rousset lithologic unit) is composed of a monotonous succession of thin-bedded silty limestones and sandstones, sometimes bioclastic with gastropods (Potamides), bivalves, and stromatolite intraclasts (F3). It is classically interpreted as a low-energy, anoxic to dysoxic shallow environment, with brackish conditions. It is followed by bioclastic rudstones and fine-grained quartz-rich packstones particularly rich in Bryozoan debris, associated with coral debris and mixed bioclasts (F9). This facies has been interpreted as the reworking and mixing of Bryozoan (Smittina) colonies formed in lower infralittoral to upper circalittoral environment. It is overlain by a thick package of marly siltstones to fine-grained sandstones rich in planktonic foraminifers (F10), deposited in low-energy, open-marine, and relatively deep conditions with episodic storm events. The upper part of this unit (Bioclastic Carry lithologic unit) comprises lobe-shaped, cross-bedded sandstones and bioclastic limestones with turritellids, bryozoans and coral-rich rudstones (F7), and two coral carpets (F8).

Finally, the fourth unit correspond to the "S-0 Aquit." sequence of Oudet et al. (2010) and to the Biodetrital Sausset lithological unit. It is dated from Aquitanian. It exhibits two sub-units made of: 1) silty, marly intervals with rare globigerinids (F10); 2) lobe-shaped quartz-rich, bioclastic limestones

(F4 and F5). The top of this unit is eroded and overlain by a marine conglomerate forming the base of the Burdigalian Plan de Sausset Unit (the latter is not included in this study).

3.3. Diagenesis overprint

A thorough diagenesis characterization of the studied succession was performed by Santerre (2010) and Hamon et al. (2013). They highlighted that sedimentary discontinuities act as major controls on the repartition of the diagenesis. Indeed, the early timing of the diagenetic modifications, the different diagenetic patterns observed in each interval and the absence of common trends in the series tend to indicate multiple episodes of early diagenesis, associated to sedimentary discontinuities. The succession may be divided into two parts: the base of the succession (Conglomeratic Rouet Unit and Parareefal Cap de Nautes Unit) and the middle-upper part of the succession (Brackish Rousset Unit, Bioclastic Carry unit, and Biodetrital Sausset-Les-Pins Unit). The basal part is dominated by diagenetic processes initiated by the mixing of seawater and meteoric water, in a proximal and restricted lagoonal setting. The middle-upper part of the succession is affected by several exposures, associated with the development of meteoric vadose and phreatic conditions. A representative example can be found at the top of the Bioclastic Carry unit (Fig. 1C), with the occurrence of a major exposure surface (SB2). This surface is associated to a well-expressed early meteoric diagenesis and has thence been selected as the target for the reactive transport modeling.

This surface affects the top of a 7 m thick coral-dominated package (F7 and F8) and consists of an angular unconformity with mean angles of dip varying from 9° to 3° across the surface (Oudet et al., 2010). Several decimetric reliefs are observed and filled by the overlying grey to ochre fine sandstones of facies F2. The surface itself shows a reddish, oxidized aspect and some detrital sediments (quartz and urgonian limestone clasts) are present between the coral colonies of facies F8. Partial or complete dissolution of corals may occur below the surface, and the created moldic

porosity is filled by a fine sandstone with a clayey, silty matrix (Facies F2). Numerous small-scale fissures (centimetric width, with a few decimeters of penetration depth, and a few decimeters to one meter of lateral extent have been observed. They affect indifferently the intra- and inter-colony sediment of the coral colonies. Two different infilling of these fissures co-occur: a blocky non-ferroan calcite cement and a fine sandstone derived from the overlying bed. Neomorphism phenomena are particularly intense below the surface and expressed in two ways: 1) recrystallization of micrite to microsparite, composed of subeuhedral crystals slightly inferior to 5 μm in size and showing a fused aspect, with no microporosity; 2) replacement of mineralogically-unstable allochems (aragonite and high-magnesium calcite/HMC), mainly displaying a fine microsparitic fabric, with dirty inclusion-rich low-magnesium calcite/LMC crystals. From a petrographic point of view, this cement is a non-ferroan and non-luminescent calcite. Both the recrystallization and the replacement decrease vertically, in the 3 to 5 m thick interval below the discontinuity. In this interval, dissolution of aragonitic bioclasts follows an opposite trend. The created moldic porosity is partially or totally filled by a drusy to blocky non-ferroan calcite (crystal size between 100 and 500 μm), non-luminescent in the topmost part of the interval, changing downward to a concentric-zoned cement with thin bright orange luminescent bands similar to the older banded cement (OBC) of Meyers (1991). Micrite recrystallization, replacement, dissolution and OBC are typical features of meteoric conditions. The results of the diagenetic study performed by Hamon et al. (2013) have been used as constraints for the validation of the modeling phase.

4. Stratigraphic forward modeling with Dionisos$^{\mathbf{Flow}}$

4.1. Input parameters

Zone of interest – Domain definition

The geological data, combining onshore sedimentological descriptions and offshore seismic data, cover an area of 10x15 km^2 (red rectangle in Fig. 1B). However, for modeling purpose, we extended this zone in order to benefit from the paleogeographic reconstructions available at larger scale from Oudet (2008), and to position more accurately the sediment sources (blue rectangle in Fig. 1B). The size of the model is therefore 40x25 km^2, with a cell size of 500x500 m^2 and a time step of 100 ky. The total duration represented by the stratigraphic model is 9.8 My, with a beginning of simulation at 23.6 My and an end at 13.8 My (Upper Oligocene - Lower Miocene).

Map of initial topography and subsidence maps

The initial topography map corresponds to the elevation of the substratum just before the beginning of the studied succession at 23.6 My. This surface corresponds to a basal unconformity, affecting Lower Cretaceous limestones of the Nerthe Massif on the North and potential Lower Oligocene (Rupelian) continental deposits in the Bay of Marseille (e.g. Fournier et al., 2016). The initial bathymetry is set above 0 m on almost the whole model, as the substratum is exposed at the beginning of the sedimentary succession and the first deposits correspond to continental facies. Maximum of altitude is around 200 m and correspond to relief surrounding the subsiding area (Figure 3). Subsidence maps correspond to the position of the substratum at selected intermediate ages. In our case study, four maps have been generated, one for each sequence boundary.

These maps are based on 3D reconstructions of a seismic dataset, integrating three sources of information: 1) low resolution, old industrial seismic data; 2) high resolution, shallow seismic data that have been previously acquired offshore Carry-le-Rouet; 3) available onshore outcrops and geologic maps. We used the available seismic interpretations from Oudet (2008), Oudet et al. (2010) and Fournier et al. (2016), that were cross-checked with onshore outcrops to obtain a consistent onshore-offshore link. The identification of the reflectors was mostly based on the stratigraphic

relationships of the different units and on seismic morphologies (Oudet et al., 2010). Then, we compiled depth points for the different horizons, which come either from local, high-resolution seismic profiles or low-resolution seismic interpretations. The conversion from reflection time to depth used the simplified velocity model proposed by Oudet (2008). The different subsidence maps were then extrapolated from these point sets and qualitatively modified to ensure a consistency with paleogeographic reconstructions by comparing location of the main depocenters and main reliefs.

Accommodation space

Accommodation space in the model is defined using (1) a set of subsidence/uplift maps that characterizes the substratum elevation at different key ages, and which were defined from a backstripping of the seismic horizons; and (2) a sea-level curve.

Through a series of trial and error runs, the average subsidence rate were set to vary from 15 m/My to 87 m/My, based on average subsidence rate in rift settings proposed by Hiscott et al. (1990) for the Mesozoic rift basins of North Atlantic (50 to 100 m/My) or Person and Garven (1992) for the Rhine graben (50 m/My). The two first units correspond to the beginning of the syn-rift phase, characterized by a high tectonic subsidence (respectively 31 and 87 m/My). On the contrary, Units 3 and 4 show lower subsidence corresponding to the end of the syn-rift and transition to post-rift phase (respectively 15 and 23 m/My).

The sea-level curve used in the model was firstly based on the eustatic curve of Haq, which represents global second and third-order sea level fluctuations (cycle duration about 0.5 to 5 My). In order to reflect the specific local paleogeography (termination of a narrow, protected gulf) and local tectonic effects, some minor modifications to this global curve were adapted to represent more accurately the duration and importance of the exposure events, observed onshore. The duration of these exposure phases has been estimated by Oudet et al. (2010) using biostratigraphy and magnetostratigraphy.

Carbonate production and siliciclastic input

In Dionisos^{Flow}, the facies classification corresponds to the final step of the simulation. It is based on the fraction of each sediment class present in each cell, which is mainly controlled by depositional parameters such as water depth and wave energy. It is thus necessary to describe the sedimentary influx in terms of sediment classes, for carbonates as well as for siliciclastic sediments. The classes considered in our model are: bioconstructed carbonates (mostly in-situ reefal carbonates), carbonate grains (bioclasts) and carbonate muds (micrite) on the one hand, conglomerate, sand, and shale on the other hand.

Carbonate production was controlled by two main parameters: water depth and wave energy. Different production-depth profiles were tested with variation of the bulk production rates per sequences. These production rates were estimated based on the facies composition (biotic and abiotic components) and bibliographic data. As shown by Schlager (2000) and Schlager (2003), due to the episodic, pulsating nature of sedimentation, carbonate production rates tend to decrease as the time span of observation increases, which make difficult the direct use of modern production rate, considering the modeling time step of 100 kyr. Therefore, we rather considered the lowest endmembers of modern production rates or accumulation rates of ancient systems.

The production of the carbonate grain sediment class was difficult to define. Even if the Aquitanian climate was tropical to subtropical (Akgün et al., 2007), the dominant grains observed in the succession are benthic foraminifers, bivalves and red algae, lacking green algae or non-skeletal grains (lumps, ooids), which are components rather associated to foramol carbonate systems. Moreover, the production rate decrease because of the mixing with siliciclastic sedimentation (Simone and Carannante, 1988; Leinfelder et al., 2004). Nelson (1978) estimated a maximum global production rate of 0,05 mm/yr for a Cenozoic carbonate shelf dominated by benthic foraminifers, bryozoan, echinoderms, and bivalves, with a significant content of terrigenous material. Collins (1988) proposed a global production rate of 0,5 mm/yr for a Holocene, non-tropical carbonates

formed of red algae, bryozoans, and lime mud, with subordinate benthic foraminifers and a low terrigenous input. These estimations are in line with the ones of Smith and Nelson (2003) for Tertiary temperate carbonates of Australia and New Zealand (0.01 to 0.1 mm/yr) and also of Read et al. (1991) who compiled modern sedimentation rates of tropical carbonates in bays with various terrigenous inputs comprised between 0.04 mm/yr and 0.4 mm/yr (Florida Bay, Carrie Bow Cay in Belize). We therefore set the production rates for carbonate grains used in the modeling between 0.02 mm/yr (unit 1) to 0.07 mm/yr (unit 4), in a range of bathymetry comprised between 0 to 20 m.

Bioconstructed carbonates (reefal carbonates dominated by coral and red algae) are generally associated with the highest production rates. Vertical reef accretion rate for modern tropical reefs averages 5.05 mm/yr (Belize, Maldives, French Polynesia; Gischler and Hudson, 2019), with a background sedimentation adjacent to the reef averaging 0.89 mm/yr. Maximum values up to 20 mm/yr for the modern Tahiti reef (French Polynesia) have been proposed by Seard et al. (2013). Smith and Nelson (2003) compiled accumulation rates for quaternary tropical shallow reefs comprised between 1 to 11 mm/yr, in line with values proposed by Read et al. (1991), comprised between 0.8 mm/yr to 3 mm/yr. Finally, considering a time integration on an interval of 100 kyr (modeling time step), Schlager (2000) or Enos (1991) estimated a range of carbonate accumulation rate under tropical conditions between 0,01 to 1 mm/yr. We therefore set the production rates for bioconstructed carbonates used in the modeling, from 0.1 (unit 1) to 0.9 mm/yr (units 3 and 4), in a range of bathymetry comprised between 0 to 5 m (Schlager, 2003). In Dionisos^{Flow}, production rates can be modulated by wave energy so that carbonate production may only be active in a specific wave-energy range. This dependency was activated for the production of the bioconstructed carbonate sediment class.

Finally, the production rates given in the literature for carbonate mud are highly variable. Read et al. (1991) proposed a range of 0,02 mm/yr to 0.1 mm/yr for outer-shelf mud (tropical conditions) mud, in line with the estimations of mud production on modern carbonate platform (Enos, 1977 and

Halley et al., 1977 for tropical platform). Blom and Alsop (1988) estimated a maximum production of 0,1 mm/yr for carbonate mud on non-tropical shelf. The production rates for carbonate mud were therefore set from 0.01 mm/yr (unit 1) to 0.04 mm/yr (units 3 and 4), in a range of bathymetry from 0 to 30 m.

Siliciclastic supply has also been estimated using the facies composition, thicknesses and duration of each unit. Based on Oudet (2008), three sources were considered, two coming from the northeastern part of the modeled area (paleo-Durance and Marseille Basin; S1 and S2 on Fig. 3) and a last one coming from the northwest (northwestern termination of the Nerthe Basin and possible secondary pathway for the paleo-Durance; S3 on Fig. 3). The total supply (resulting from the three sources) varies from 0.5 to 3 km^3/My. The nature of the sedimentary load and the sedimentary supply are also variable and depend on the source and the stratigraphic units.

Sediment transport

Sediment transport can be modeled with Dionisos^{Flow} by a long-term water- and slope-driven diffusion equation (Granjeon & Joseph, 1999). The corresponding parameters are presented in Table 2. The wave propagation angle was set as coming from the southwest (opening of the gulf) and the wave base was set at 20 m with a maximum of energy around 10 m of bathymetry.

4.2. Simulation results

The construction of the model was based on independent tests on the two main parameters controlling basin sedimentation: 1) competition between carbonate production and siliciclastic supply; 2) subsidence (sea-level curve). Eleven experiments were performed, by changing one parameter at a time while keeping the others constant. The results of these simulations were validated qualitatively by comparison between the modeled facies distribution (relative proportions of carbonate vs. siliciclastic sediments) and paleogeography, and the conceptual sedimentary model.

Quantitatively, the thickness of the deposits and their geometry, as well as the timing of reef geographic distribution, were compared with the stratigraphic architecture observed on seismic profiles. These series of trial and error runs to develop the best-fit case will not be discussed here, as the objective of the paper is to use this best-fit simulation as a basis for reactive transport modeling.

The best-fit model is presented in Figure 4. The onset of modeling at 28.1 My (Late Oligocene) is associated with the start of the basement subsidence in the NW-SE gulf, which subsequently captured most of the sourced sediments. The first deposits in the center of the basin are of alluvial type, partially reworked in a shallow coastal setting (F1; 27.1 My). The basin is progressively drowned, and at 24.3 My, the Carry-Le-Rouet section is located on the seashore. There, the facies correspond to a mixing of conglomerates and sandstones (F1 and F2), with quartz-rich carbonates, deposited on a shallow inner-shelf (F4).

After a sea level drop at 23.7 My associated to sequence boundary SB0 on the Carry-Le-Rouet section, the Early Miocene transgression favors the development of inner-shelf marls (F6), bordered by shallow-inner shelf carbonates (F4; 23.3 My). Localized development of coral carpets (F8), coral-rich rudstones associated with localized scattered coral colonies (F7), and background inner- to mid-shelf sediments (F5) are also reproduced. The facies F8, that is characterized by a maximum lateral extent of a few hundreds of meters is here over-represented, which is due to the coarse grid used in the simulation, with a cell size of 500x500 m. This coarse grid also generated an artificial lateral continuity of the facies F8, which was not observed at outcrop. In a lesser extent, the distribution of the facies F7, is over-estimated for the same reason. A better representation could be produced using a finer grid resolution, but it implies a higher computation time (see discussion part). Sandstones (F2) and Potamides-rich wackestones (F3), typical of low-energy, shallow brackish conditions can be observed upstream or during lowstand. This configuration is persistent until 22.5 My, corresponding to a relative sea-level drop and the development of sequence boundary SB1.

A renewed progressive flooding occurs until 22.1 My (maximum flooding surface) due to active rifting and eustatic rise. Some transgressive distal deposits, such as mid-shelf (F9) and outer-shelf (F10) facies are recorded on the Carry section. Subsequently, the sequence progrades during the highstand, with the occurrence of facies F5 (low-energy, marine, inner- to mid-shelf (kilometric lateral extent) and localized development of coral carpets (F8).

At 21.5 My, the development of sequence boundary SB2 is marked by a general exposure, observed on the Carry section (meteoric diagenesis) and a hiatus. From 21.1 to 20.1 My, a new transgression is observed on the Carry section with the development of littoral coral-rich facies (F4 and F7), until the maximum flooding marked by the deposition of open-marine, distal facies (F9 and F10). The model ends at 18.3 My, which corresponds to the final exposure of the succession and the formation of sequence boundary SB3, after the deposition of littoral quartz-rich bioclastic wackestones to packstones during a late highstand (facies F5 and F4).

5. Reactive transport modeling with Coores-Arxim

The detailed diagenetic study of outcrop data demonstrated that the overall rock properties are mainly defined by the depositional conditions of sedimentary layers, and by a few diagenetic events such as the major sea-level drop and exposures of the sedimentary systems (Hamon et al., 2013). One of these events is recorded by the exposure surface SB2 (21.5 My), and an important sedimentary hiatus, estimated to have a duration of 800 ky by Oudet et al. (2010), associated with a meteoric diagenesis. To better evaluate how RTM could be used in combination with a SFM, we focused our reactive transport modeling on this SB2 surface and time interval.

5.1. Input parameters

Grid and simulation time

The reactive transport model was built from the geometry and facies distribution calculated by Dionisos^{Flow} at 21.5 My. Nevertheless, as reactive transport simulations are associated to very long computation times, several simplifications had to be adopted.

Firstly, geochemical calculations were not performed on the entire 3D model, but only along a 2D-section extracted from the Dionisos^{Flow} mesh. Secondly, every cell located below sea-level was considered to be water saturated, while the other ones were excluded from the reactive transport model. The resulting mesh is a 36.5 km long, 500 m large (1 cell only) and between 4 to 132 m high vertical 2D-section (Fig. 5A; Table 2). Cell size is 500 m long in X- and Y- directions and from 0.10 to 3.5 m in Z-direction. Finally, the time period covered by the reactive transport simulation is limited to about 27 ky (9.9×10^6days).

Boundary conditions

Meteoric effective recharge is modeled by a constant flow rate of 0.34 m/y imposed on the continental section of the top layer of the model (Fig. 5B; Table 2). This flow rate corresponds to a mean annual precipitation close to 1200 mm (in line with the paleoclimate estimation during the Early Miocene; Kroh, 2007), with an important run-off. The injected fluid composition corresponds to rainwater equilibrated with a 10^{-2} bar partial pressure of CO_2, in accordance with the atmosphere composition estimated by Pagani et al. (1999) for Miocene. The permeability of the substratum was considered much lower than the ones of the sedimentary pile, which was represented through a closed bottom boundary condition. The effect of groundwater venues was investigated considering influx velocities of 0, 25 or 250 m/y at the eastern boundary. The associated flow rates remain negligible when compared to the meteoric recharge, as it is applied on the eastern boundary, which represent a small portion compared to the topographic surface. It had therefore no effect on the

simulation. The results presented here have been obtained with the no-flux condition on this eastern boundary (Fig. 5B; Table 2). Finally, the western boundary and the one corresponding to the seafloor were always considered at hydrostatic pressure (Fig. 5B).

Initial conditions

The Dionisos^{Flow} facies distribution was used to define the initial conditions of the Coores-Arxim model (Fig. 5A). In that regard, it was necessary to characterize each facies in terms of reactive transport parameters (Table 1): 1) a quantitative mineralogy, derived from point counting of the different allochems on thin sections, and visual estimation of the initial mineralogy following Flügel (2004). Even if, the dominant initial phase of shallow-marine-carbonate muds is either aragonite or HMC, an initial alteration of the metastable muds producing LMC "micrites" was considered (Folk, 1965); 2) a depositional porosity, using empirical relationships with depositional textures from modern sediments (Enos and Sawatsky, 1981; Lucia, 2007), which was translated into an effective initial porosity to simulate the effect of early compaction, using a compaction law $\Phi(z)$, adapted from Ricken (1987) to take into account higher initial depositional porosity; 3) an effective initial porosity and permeability using a standard Kozeny-Carman $K(\Phi)$ relationship and a reference value of 100 mD for a porosity equal to 25%. The Kozeny-Carman relationship is usually valid for a floating sphere model, and its use is debatable for muddy textures. However, the Coores-Arxim model is based on such a floating sphere model. It obviously represents an intrinsic limitation to the modeling, but we followed here the assumptions made by Gabellone et al (2006) and Al-Helal (2012) who also used this type of relationship for such textures. Moreover, considering the many uncertainties and strong assumptions made for RTM, we considered the use of this law acceptable in this context.

In addition, this model was considered always isothermal at 25°C, initially at hydrostatic pressure with a reference pressure equal to 1 bar at the surface (depth = 0 m), and initially fully saturated with modern seawater (composition taken from Blomme et al., 2017), modified using batch geochemical modeling to be at thermodynamic equilibrium with LMC and quartz. Table 3 gives the elementary

composition of the solutions used in the reactive transport simulations to represent the initial water in the system and the rainwater invading the model.

Thermodynamic and kinetic parameters

Four minerals were considered in this study: aragonite, HMC, LMC and quartz (Table 4). The thermodynamic database used in the reactive transport simulations is SLOP98 (www.predcent.org), and the activity model for aqueous species is the B-dot model. This thermodynamic database was completed with an equilibrium constant for HMC proposed by Walter and Morse (1984). The kinetic models for dissolution of minerals are based on the USGS compilation of Palandri and Kharaka (2004). The product of aragonite kinetic constant and reactive surface area was then adjusted to achieve an approximate half-life for aragonite of 6700 years (duration estimated from field data; Vacher et al., 1990). These modified aragonite kinetic parameters were used for HMC as well. LMC and quartz were respectively attributed the original calcite and quartz kinetic models of the USGS compilation of Palandri and Kharaka (2004). It is common knowledge that precipitation kinetics are poorly constrained. As a first approach, the same kinetic models were considered for dissolution and precipitation. The latter process is nonetheless overall slower in the simulations, as the secondary minerals, initially defined as germs in very low quantities, show a much smaller reactive surface area than primary minerals. Reactive surface areas are notoriously highly uncertain parameters: previous works evaluated a difference of up to three orders of magnitude between estimated reactive surface area (laboratory experiments) and lab-measurable BET-surface area (White and Peterson, 1990; Gaus, 2005). In the absence of direct measurement methods of the reactive surface area, the classical way is to approximate it from simple geometric texture models. In the present study, a floating sphere model was used, with an initial grain radius of 100 µm and 0.01 µm for respectively primary and secondary minerals. The use of such mainstream approaches seems adequate in regard with the methodological philosophy of this work. More advanced texture models are amongst the improvements that could be made in future studies.

5.2. Simulation results

Calculation results at the end of the simulation (27 ky) show the occurrence of two domains of salinity, that were associated with two distinct diagenetic environments: marine and meteoric phreatic. This configuration is a very simplified representation of the real hydrozonation occurring in a littoral setting, with a marine wedge, overlain by mixing and meteoric environments. However, the RTM code used at the time of the study had some limitations. It was not possible to simulate: 1) the mixing zone as the density effect is not taken into account in this calculation, which explained this vertical boundary between the marine and meteoric waters; 2) the non-saturated zone, that was excluded from the reactive transport model. The calculation results are thus discussed only in the two modeled hydrozones.

Whatever the diagenetic domain, an overall stabilization of aragonite to LMC cement is observed (Fig. 6A, 6B and 6E), associated with a porosity decrease up to 3% (Fig. 6D). On the opposite, HMC remains stable and unaltered in the marine zone, whereas it is progressively dissolved and stabilized as LMC cement in the topmost part of the meteoric zone (Fig. 6C, 6D and 6E). This stabilization process is associated with a porosity increase (up to 4%) that depends on the cell proximity to the surface (Fig. 6F).

The mineralogical variations with time for two representative facies and different diagenetic environments are presented in Figure 7. The initial grain mineralogy of the coral facies (F8) is dominated by aragonite, representing coral colonies and debris. The results show that the alteration of this facies is almost identical (replacement of aragonite by LMC cement) whether it is located in the meteoric phreatic zone (graph 3 of Figure 7) or in the marine phreatic zone (graph 4 of Figure 7). This can be explained by the lesser thermodynamic stability of aragonite compared with LMC, which leads to a systematic replacement process controlled by the reaction kinetics (and thus not influenced by advective transport of species). The shallow quartz-rich bioclastic wackestone-

packstone (F4) contains initially some carbonate grains possibly made of HMC (mainly benthic foraminifera and Corallinaceae). Contrary to coral carpets (F8), F4 shows a different behavior according to the diagenetic environment. HMC is a mineral thermodynamically stable in seawater, and no mineralogical transformation is thus observed for the facies located in the marine phreatic environment (graph 4 of Figure 7). In contrast, in the meteoric phreatic zone, progressive dissolution of HMC and replacement by an LMC cement are observed. Replacement is pronounced in the first line of cells below the topographic surface (graph 1 of Figure 7) and tends to decrease with depth (graph 2 of Figure 7). In fact, the rainwater entering the model is undersaturated with respect to LMC, and thus induces dissolution processes in the immediate vicinity of the topographic surface, that is the most exposed to meteoric recharge (Figure 7). This also highlights the important role played by transport of chemical species in this process. Indeed, rainwater reaching buried cells containing HMC has partly reacted along its migration path and is therefore less prone to cause mineralogical destabilization.

6. Discussion

6.1. Mineralogical transformations

Due to the dynamic nature of a sedimentary basin and the relatively small period covered by the reactive transport simulation, only a qualitative evaluation of the numerical results is possible. Regarding the mineralogical reactions, the quality of the model was evaluated by comparing numerical results with petrographic observations characteristic of either marine or meteoric phreatic zones (Hamon et al., 2013). The decreasing trend of replacement and matrix recrystallization observed downward from the exposure surface (Fig. 8A) is notably correctly reproduced in the simulation (Fig. 6C). The development of an important neomorphism immediately below the surface is also observed. It can contribute significatively to form porosity/permeability barriers and generate

reservoir compartmentalization. Such barriers have been described on other real case studies (James, 1972; Wendte and Muir, 1995; Wagner et al., 1995).

Petrographic observations of thin sections coming from the presumed meteoric phreatic zone showed that neither aragonite nor HMC is preserved. In addition, dissolution of HMC seems to systematically lead to porosity creation. These observations are in line with simulation results. On the contrary, some discrepancies with the aragonite behavior are observed. In the simulation, the dissolution of aragonite is compensated by the precipitation of LMC in the same cell, and no or very little porosity is created (Fig. 8B). However, in thin sections, aragonite is not always replaced by a LMC cement and moldic porosity may be observed (Fig. 8C). As indicated by Moore (2001), the rate of calcite growth from a solution in equilibrium with aragonite is at least 100 times slower than the rate at which aragonite will dissolve. This large kinetic difference between aragonite dissolution and calcite precipitation implies that the species liberated in solution by aragonite destabilization are generally transported away from the reaction sites. This observation highlights the sensitivity of some diagenetic processes to kinetic effects, unfortunately poorly constrained in reactive transport simulations.

Petrographic observations of thin sections (made by Hamon et al., 2013) of samples not affected by meteoric diagenesis, at the base of the sedimentary succession, revealed that some HMC bioclasts are preserved (Fig. 8D and 8E), whereas aragonite ones are not, which is in line with simulation results. The preservation or dissolution of HMC in the marine environment is a matter of debate. Some uncertainties remain on its intrinsic thermodynamic parameters. The variable composition of HMC, that may contain from 2 to 24 mole % of Mg, induces changing solubility (Plummer and Mackenzie, 1974; Morse and Mackenzie 1990) and thus different behavior. According to the results of Morse et al. (2006), the solubility of HMC is a function of the molar content of $MgCO_3$ and it can exceed that of aragonite. Thus, in modern tropical environments, HMC can be dissolved or preserved

(metastable state) (Haese et al., 2014) and can even be preserved in case studies of ancient systems (Stanienda-Pilecki, 2018).

6.2. Input parameters and scale compatibility

This work aimed at exploring the possibility to couple SFM and RTM at basin-scale. The objective was methodological, and the study aimed at identifying the difficulties to use RTM in combination with a classical SFM approach. As demonstrated in this study: 1) 3D SFM simulations reproduced adequately the facies distribution and sedimentary architectures; 2) 2D RTM simulations provided correct overall trends and spatial distribution, but with discrepancies and inaccurate discrete values (porosity, percentage of the different mineral phases) compared to the present-day measured values. One can discuss if these results can be generalized to other case studies and in which conditions.

Present-day rock properties (mineralogy, porosity, and permeability) are representative of a cumulative diagenetic history, with eogenetic and mesogenetic modifications. However, when the petrophysical properties are mainly driven by the facies and one specific diagenetic event, it seems possible to rely on the SFM-RTM simulation to describe the main diagenetic and petrophysical trends.Hamon et al. (2013) demonstrated that the studied sedimentary succession underwent a low burial depth and that overall rock properties were mainly defined by the eogenetic modifications associated to exposures of the sedimentary systems, well-reproduced by our modeling approach. In the same way, Gabellone et al. (2016) reproduced an overall correct pattern of dolomitization due to brine reflux, this dolomitization being one major diagenetic driver of the petrophysical properties (Barbier et al, 2015).

Even if RTM is theoretically applicable across a great range of scales (Xiao and Jones, 2006), SFM and RTM are generally poorly compatible in terms of space and time scale. Indeed, SFM usually deals with characteristic time scale (time step) of 100 ky to 1 My and characteristic space scale (cell size) of

hundreds of meters to several kilometers, whereas RTM is associated with finer grid cells and time steps. The combined use of SFM and RTM thus requires some simplifications to make both descriptors compatible. Particularly, it is important to better understand how to characterize the facies modeled by SFM at basin-scale, in terms of textural, mineralogical and petrophysical properties and how to define the fluids used as inputs in RTM.

The first question is how SFM translates sedimentary processes into first-order physics to characterize sedimentary systems, in 3D, at basin to appraisal scales (Granjeon and Joseph, 1999). This implies an upscaled, low-resolution representation of the heterogeneities of textural, mineralogical and petrophysical properties, as each cell is the equivalent of several sedimentary facies. Upscaling and downscaling problems are well-known in subsurface modeling and simulations and lot of work has been dedicated to these questions (Renard and de Marsily, 1997; Blöschl and Sivapalan, 1995; Durlofsky, 2002; Noetinger and Zargar, 2004; Noetinger et al., 2005; Qi and Pei, 2008; Mikes, 2011; among others). However, most of them deal with facies heterogeneities and only a few works have been done in upscaling-downscaling issues of quantification of mineral data (Butcher, 2020). In our case study, we thus considered stabilized LMC micrite and estimated the effective initial porosity, derived from the depositional porosities and the compaction effect occurring in the first 10s centimeters to few meters of the sedimentary pile. Simplifications of the depositional texture were also mandatory, with the use of a floating spheres texture model in Coores-Arxim. This last point is problematic to accurately represent the complex carbonate textures, particularly for boundstone textures or for mixed textures (wackestone, packstone) that may affect the diagenetic process through the combined control of fluid flux and effective reactive surface area (Gabellone and Whitaker, 2016). All these considerations may explain some of the inaccuracies in our simulations, even if the general trends are honored.

The second question deals with the definition of the fluid geochemistry used as inputs in RTM. Here, the most reasonable hypotheses are considered, given the information we have from the fossil

record (modern rainwater at equilibrium with Miocene atmospheric pCO_2, modern seawater equilibrated with the most stable primary minerals). Residence time of each cell in each hydrozone can also be estimated using a groundwater model, integrated in Dionisos^{Flow}. Again, this seems enough to reproduce correct trends at basin-scale, but insufficient to obtain a fully calibrated model. Moreover, at the basin-scale several high-order sea level variations and exposures could develop, leading to additional high-order water composition variations and difficulties to precisely reproduce the actual data (such as petrographic observations).

This work illustrates how the simulation results are conditioned by the accuracy of the input, themselves controlled by both the model space and time scale. This preliminary, mainly methodological study implied simplified parameters and the use of a coarse-, low-resolution, SFM grid, that can be considered adequate to test our geological hypotheses at basin-scale, but insufficient to reproduce detailed heterogeneities at a finer scale. The use of a higher grid resolution (cell size of 100x100 m) may help to bridge the gap between SFM and RTM, but it implies a much higher computation time (from 35 minutes to 2 hours for SFM and from 5 hours to more than a day for RTM). This increase of the computation time can be partly attenuated for SFM using a larger time step of 20 ky, but not for RTM, as it is fixed by the software. At reservoir-scale, alternative methods exist, as for example the use of the SFM model as framework for detailed geostatistical lithofacies and petrophysical modeling in a finer, high-resolution grid (Doligez et al., 1999; Sacchi et al. 2016). Such an approach can help to tackle the scaling issues and enables to propagate and quantitatively assess the uncertainty associated with each SFM parameter. The main drawback of such geostatistical approaches is that the diagenetic reactions are only represented by their effect on reservoir properties and are not explicitly modeled. A 3D quantitative geochemical calculation at the scale (both in space and time) of a Dionisos^{Flow} model is still out of reach due to important computation time. Such a combination has a lot of potential for the future to better characterize diagenetic overprints at basin and reservoir scale. This will significantly improve our reservoir

characterization and modeling capacities and the presented work constitutes a first step in this direction.

7. Conclusion

The approach proposed in this article is based on modeling, using a combined approach: 1) firstly a 3D stratigraphic forward model (Dionisos^{Flow}) to simulate the Upper Oligocene - Lower Miocene, mixed siliciclastic-carbonate shelf system that developed in the northern termination of the Liguro-Provençal Basin; 2) secondly a 2D reactive transport model (Coores-Arxim) at a key geological age characterized by a major sea-level drop and exposure, to represent the associated meteoric diagenesis.

The Dionisos^{Flow} model is based on a 40x25 km^2 grid with a cell size of 500x500 m and a time step of 100 ky. Three stratigraphic units are modeled, consisting of shallow carbonates mixed with important fluvial siliciclastic inputs. The model reproduced adequately the main sedimentary trends, namely the facies distribution, the thickness of the deposits and the sedimentary architectures, but failed to represent accurate fine-scale sedimentary heterogeneities, such as localized small-scale coral carpets that are below the model resolution. This study demonstrates that Dionisos^{Flow}, which is generally used to simulate the long-term and large-scale evolution of sedimentary basins, can also be considered as a reliable tool to model shallow carbonate systems, even in a complex mixed sedimentary setting, where competition between siliciclastic and carbonate sedimentation occurs.

The Coores-Arxim calculations aimed at modeling the early meteoric diagenesis associated to a major exposure of the succession, and its marine counterpart where the shelf remained submerged. Processes of dissolution, recrystallization, cementation and resulting petrophysical evolutions were examined. The simulations presented here provide a correct representation of the observed diagenetic trends, as they are, at least qualitatively, in agreement with the petrographic

observations. An exception is the replacement of aragonite by a calcite cement, that systematically occurred in the model and is not always observed in thin sections.

This methodological study provided some interesting and consistent low-resolution diagenetic and petrophysical trends, at large-scale. It emphasizes the issues associated with the parameter definition and scale mismatch of the two modeling approaches, that preclude an accurate quantification of the resulting properties (porosity, permeability) at finer scale. However, it is a first step toward a full 3D integration of geochemical calculations in stratigraphic forward model, that represent a challenging and promising R&D topic.

8. Acknowledgments

We thank two anonymous reviewers and the Guest Editor Dr. Sara Tomás for their constructive comments and suggestions, that considerably improved the original manuscript.

9. References

Akgün, F., Kayseri, M.S., Akkiraz, M.S., 2007. Palaeoclimatic evolution and vegetational changes during the Late Oligocene–Miocene period in Western and Central Anatolia (Turkey). Palaeogeography, Palaeoclimatology, Palaeoecology 253(1-2), 56-90.

Al-Helal, A.B., Whitaker, F.F., Xiao, Y., 2012. Reactive transport modeling of brine reflux: dolomitization, anhydrite precipitation, and porosity evolution. Journal of Sedimentary Research 82, 196-215.

Andreieff, P., Anglada, R., Carbonnel, G., Catzigras, F., Cavelier, C., Chateauneuf, J.J., Colomb, E., Glintzboeckel, C., Jacob, C., Lai, J., L'Homer, A., Lezaud, L., Lorenz, C., Mercier, H., Parfenoff A., 1972. Contribution à l'étude de Carry-le-Rouet (Bouches-du-Rhône). Cinquième congrès du Néogène Méditerranéen, Mémoire du BRGM 3, 132 p.

Ayora, C., Taberner, C., Saaltink, M.W., Carrera, J., 1998. The genesis of dedolomites: a discussion based on reactive transport modelling. Journal of Hydrology 209(1), 346-365.

Bachaud, P., Meiller, C., Brosse, E., Durand, I., Beaumont, V., 2017. Modeling of hydrogen genesis in ophiolite massif. 15th Water-Rock Interaction International Symposium, WRI-15. Procedia Earth and Planetary Science 17, 265-268.

Bache, F., 2008. Evolution Oligo-Miocène des marges du micro-océan Liguro-Provençal. PhD thesis, Univ. Bretagne Occidentale, 338 p.

Barbier, M., Hamon, Y., Doligez, B., Callot, J.-P., Floquet, M., Daniel, J.-M., 2012. Stochastic joint simulation of facies and diagenesis: A case study on early diagenesis of the Madison formation (Wyoming, USA). Oil & Gas Science and Technology 67(1), 123-145.

Barbier, M., Floquet, M., Hamon, Y., Callot, J.-P, 2015. Nature and distribution of diagenetic phases and petrophysical properties of carbonates: The Mississippian Madison Formation (Bighorn Basin, Wyoming, USA). Marine and Petroleum Geology 67, 230-248.

Berra, F., Lanfranchi, A., Smart, P.L., Whitaker, F.F., Ronchi, P., 2016. Forward modeling of carbonate platforms: Sedimentological and diagenetic constraints from an application to a flat-topped greenhouse platform (Triassic, Southern Alps, Italy). Marine and Petroleum Geology 78, 636-655.

Blázquez-Fernández, S., López-Cilla, I., Gasparrini, M., Rosales, I., Lerat, O., Doligez, B., Martín-Chivelet, J., 2013. Approaches to model and predict facies/texture/porosity interdependence in a dolomitised Urgonian platform (Western Basque-Cantabrian Basin, Spain). IAS 30th Meeting, Manchester, England, 2-9 September.

Blom, W.M., Alsop, D.B., 1988. Carbonate mud sedimentation on a temperate shelf: Bass Basin, Southeastern Australia. Sedimentary Geology 60, 269-280.

Blomme, K., Fowler, S.J., Bachaud, P., Nader, F.H., Michel, A., Swennen, R., 2017. Ferroan Dolomitization by Seawater Interaction with Mafic Igneous Dikes and Carbonate Host Rock at the Latemar Platform, Dolomites, Italy: Numerical Modeling of Spatial, Temporal, and Temperature Data. Geofluids 2017, Article ID 6590672, 1-14.

Blöschl, G., Sivapalan, M., 1995. Scale issues in hydrological modelling: A review. Hydrological Processes 9(3-4), 251-290.

Burgess, P.M., Lammers, H., van Oosterhout, C., Granjeon, D., 2006. Multivariate sequence stratigraphy: tackling complexity and uncertainty with stratigraphic forward modelling, multiple scenarios and conditional frequency maps. AAPG Bull. 90, 1883-1901.

Butcher, A.R., 2020. Upscaling of 2D mineralogical information to 3D volumes for geoscience applications using a multi-scale, multi-modal and multi-dimensional approach. IOP Conf. Series: Materials Science and Engineering 891, 1-7.

Carrera, M.F.L., Barbier, M., Le Ravalec, M., 2018. Accounting for diagenesis overprint in carbonate reservoirs using parametrization technique and optimization workflow for production data matching. Journal of Petroleum Exploration and Production Technology 8, 983-997.

Caspard, E., Rudkiewicz, J.L., Eberli, G.P., Brosse, E., Renard, M., 2004. Massive dolomitization of a Messinian reef in the Great Bahama Bank: a numerical modelling evaluation of Kohout geothermal convection. Geofluids 4(1), 40-60.

Chevalier, J.P., 1961. Recherches sur les madréporaires et les formations récifales Miocènes de la Méditerranée occidentale. Mémoires de la Société Géologique de France, Nouvelle Série, 93, 562 p.

Collins, L.B., 1988. Sediments and history of the Rottnest Shelf, southwest Australia: a swell-dominated, non-tropical carbonate margin. Sedimentary Geology 60 (1-4), 15-49.

Conesa, G., Demory, F., Le Doussal, C., Londeix, L., Pagès, J.-S., 2014. L'Aquitanien en France. In: Londeix L. (Ed.), Stratotype Aquitanien Collection Patrimoine géologique, Muséum national d'Histoire naturelle, Paris, 415 p.

Conesa, G., Demory, F., Oudet, J., Cornée, J.J., Münch, P., Rubion, J.L., 2005. L'Oligo-Aquitanien de la Côte Bleue : les systèmes récifaux et bioclastiques du littoral méditerranéen entre l'Estaque et la Couronne. In: Parize, O., Rubino, J.-L. (Eds.), Les systèmes oligo-miocènes carbonatés et clastiques de Basse-Provence. Des témoins de l'évolution géodynamique de la marge provençale et du bassin d'avant-pays alpin. Livret guide Excursion E8/E9 du Xème Congrès ASF, presqu'île de Giens, 7-16 octobre 2005, 55-77.

Consonni, A., Ronchi, P., Geloni, C., Battistelli, A., Grigo, D., Biagi, S., Gherardi, F., Gianelli, G., 2010. Application of numerical modelling to a case of compaction-driven dolomitization: a Jurassic palaeohigh in the Po Plain, Italy. Sedimentology 57(1), 209-231.

Cooper, K., Whitaker F., Rudd, M., Hemmings B., 2004. Reactive transport modelling the early meteoric diagenesis of a carbonate island: a critical consideration of complexity. Goldschmidt Conference 2014, Sacramento, California, 8-13 June.

Csato, I., Tóth, S., Catuneanu, O., Granjeon, D., 2015., A sequence stratigraphic model for the Upper Miocene-Pliocene basin fill of the Pannonian Basin, eastern Hungary. Marine and Petroleum Geology 66, 117-134.

De Boever, E., Varloteaux, C., Nader, F.H., Foubert, A., Békri, S., Youssef, S., Rosenberg, E., 2012. Quantification and Prediction of the 3D Pore Network Evolution in Carbonate Reservoir Rocks. Oil & Gas Science and Technology 67(1), 161-178.

Demory, F., Conesa, G., Oudet, J., Mansouri, H., Münch, P., Borgomano, J., Thouveny, N., Lamarche, J., Gisquet, F. and Marié, L., 2011. Magnetostratigraphy and paleoenvironments in shallow-water carbonates: the Oligocene-Miocene sediments of the northern margin of the Liguro-Provençal Basin (West Marseille, southeastern France). Bulletin de la Société Géologique de France 182, 37-55.

Deville, E., Mascle, A., Callec, Y., Huyghe, P., Lallemant, S., Lerat, O., Mathieu, X., De Carillo, C.P., Patriat, M., Pichot, T., Loubrieux, B., Granjeon, D., 2015. Tectonics and sedimentation interactions in the east Caribbean subduction zone. An overview from the Orinoco delta and the Barbados accretionary prism. Marine and Petroleum Geology 64, 76-103.

Doligez, B., Granjeon, D., Joseph, P., Eschard, R., Beucher, H., 1999. How can stratigraphic modeling help constrain geostatistical reservoir simulations? ". In: Harbaugh, J.W., Watney, W.L., Rankey, E.C.,

Slingerland, R., Goldstein, R.H., Franseen, E.K. (Eds). Numerical Experiments in Stratigraphy: Recent Advances in Stratigraphic and Sedimentologic Computer Simulations, SEPM Sp. Publ. 62, 239-244.

Durlofsky, L.J., 2002. Upscaling of Geological Models for Reservoir Simulation: Issues and Approaches. Computational Geosciences 6, 1-4.

Enos, P., 1977. Holocene sediment accumulations of the South Florida shelf margin. In: Enos P., Perkins R.D. (Eds), Quaternary Sedimentation in South Florida, Geological Society of America, Memoir, 147, 1-130.

Enos, P., 1991. Sedimentary parameters for computer modeling. Kansas Geological Survey Bulletin 233, 63-99.

Enos, P., Sawatsky, L.H., 1981. Pore networks in Holocene carbonate sediments, Journal of Sedimentary Petrology 51(3), 961-985.

Estublier, A., Fornel, A., Parra, T., Deflandre, J. P., 2013. Sensitivity study of the reactive transport model for CO2 injection into the Utsira saline formation using 3D fluid flow model history matched with 4D seismic, Energy Procedia 37, 3574-3582.

Flügel, E., 2004. Microfacies of Carbonate Rocks. Springer, New York, 976 p.

Folk, R.L., 1965. Some aspects of recrystallization in ancient limestones. In: Pray, L.C., Murray, R.C. (Eds.), Dolomitization and limestone diagenesis. A symposium. SEPM (Society for Sedimentary Geology) Special Publication 13, 14-48.

Fournier, F., Tassy, A., Thinon, I., Münch, P., Cornée, J.-J., Borgomano, J., Léonide, P., Beslier, M.-O., Fournillon, A., Gorini, C., Guennoc, P., Oudet, J., Rabineau, M., Sage, F., Toullec, R., 2016. Pre-Pliocene tectonostratigraphic framework of the Provence continental shelf (eastern Gulf of Lion, SE France). Bulletin de la Société Géologique de France 187(4-5), 187-216.

Gabellone, T., Whitaker, F., 2015. Secular variations in seawater chemistry controlling dolomitizationdolomitisation in shallow reflux systems: insights from reactive transport modelling. Sedimentology 63, 1233-1259.

Gabellone, T., Whitaker, F., Katz, D., Griffiths, G., Sonnenfeld, M., 2016. Controls on reflux dolomitizationdolomitisation of epeiric-scale ramps: insights from reactive transport simulations of the Mississippian Madison Formation (Montana and Wyoming). Sedimentary Geology 345, 85-102.

Galloni, F., 2003. Organisation sédimentaire et anatomies récifales des systèmes carbonatés à silicoclastiques Oligo-Miocènes inférieurs de Provence et du bloc corso-sarde. PhD Thesis, Provence University, France, 300 pp.

Gattacceca, J., Deino, A., Rizzo, R., Jones, D.S., Henry, B., Beaudoin, B., Vadeboin, F. (2007). Miocene rotation of Sardinia: New paleomagnetic and geochronological constraints and geodynamic implications. Earth and Planetary Science Letters 258(3-4), 359-377.

Gaus, I., Azaroual, M., Czernichowski-Lauriol, I., 2005. Reactive transport modelling of the impact of CO2 injection on the clayey cap rock at Sleipner (North Sea). Chemical Geology 217, 319-337.

Gischler, E., Hudson, J.H., 2019. Holocene tropical reef accretion and lagoon sedimentation: A quantitative approach to the influence of sea-level rise, climate, and subsidence (Belize, Maldives, French Polynesia). The Depositional Record 5, 515-539.

Granjeon, D., 1997. Modélisation stratigraphique déterministe : conception et applications d'un modèle diffusif 3D multilithologique. PhD Thesis, University of Rennes 1, France, 175 p.

Granjeon, D., 2014. 3D stratigraphic forward model compared with analogue flume model: insights on the non-linear water-driven sediment transport and on the impact of baselevel cycles on continental margin and incised valleys. In: Martinius, A.W., Ravnas, R., Howell, J.A., Steel, R.J., Wonham, J.P. (Eds), From depositional systems to sedimentary successions on the Norwegian continental margin. IAS Special Publication 47, 453-472.

Granjeon, D., Joseph, P., 1999. Concepts and applications of a 3D multiple lithology, diffusive model in stratigraphic modeling. In: Harbaugh, J.W., Watney, W.L., Rankey, E.C., Slingerland, R., Goldstein R.H., Franseen E.K. (Eds.), Numerical Experiments in Stratigraphy: Recent Advances in Stratigraphic and Sedimentologic Computer Simulations, (Society for Sedimentary Geology) Special Publication 62, 197-210.

Haese, R.R., Smith, J., Weber, R., Trafford, J., 2014. High-Magnesium Calcite Dissolution in Tropical Continental Shelf Sediments Controlled by Ocean Acidification. Environ. Sci. Technol. 48(15), 8522-8528

Halley, R.B., Shinn, E.A., Hudson, J.H., Lidz, B., 1977. Recent and relict topography of Boo Bee patch reef, Belize. 3rd International Coral Reef Symposium, 2, Miami, 29-35.

Hamon, Y., Deschamps, R., Joseph, P., Doligez, B., Schmitz, J., Lerat, O., 2016. Integrated workflow for characterization and modeling of a mixed sedimentary system: The Ilerdian Alveolina Limestone Formation (Graus-Tremp Basin, Spain). Comptes-Rendus Géosciences 348(7), 520-530.

Hamon, Y., Santerre, Y., Granjeon, D., Conesa, G., Borgomano, J., 2013. Early diagenesis in meteoric versus brackish environments: Example of the Late Oligocene – Early Miocene sedimentary succession of Carry-le-Rouet (Southeastern France). Bulletin de la Société Géologique de France 184(6), 601-620.

Hiscott, R.N., Wilson, R.C. L., Gradstein, F.M., Pujalte, V., García-Mondéjar, J., Boudreau, R.R., Wishart, H.A., 1990. Comparative stratigraphy and subsidence history of Mesozoic rift basins of north Atlantic. AAPG Bulletin 74, 60-76.

James, N.P., 1972. Holocene and Pleistocene Calcareous Crust (Caliche) Profiles: Criteria for Subaerial Exposure. Journal of Sedimentary Petrology 42(4), 817-836.

Kolodka, C., Vennin, E., Bourillot, R., Granjeon, D., Desaubliaux, G., 2016. Stratigraphic modelling of platform architecture and carbonate production: A Messinian case study (Sorbas Basin, SE Spain). Basin Research 28(5), 658-684.

Kroh, A., 2007. Climate changes in the Early to Middle Miocene of the Central Paratethys and the origin of its echinoderm fauna. Palaeogeography, Palaeoclimatology, Palaeoecology 253(1-2), 169-207.

Lanteaume, C., Fournier, F., Pellerin, M., Borgomano, J., 2018. Testing geologic assumptions and scenarios in carbonate exploration: Insights from integrated stratigraphic, diagenetic, and seismic forward modeling. The Leading Edge 37(9), 634-712.

Lantuéjoul, C., 2001. Geostatistical simulation: models and algorithms. Springer, Berlin, 256 p.

Lasaga, A. C., 1984. Chemical kinetics of water-rock interactions. Journal of Geophysical Research 89(B6), 4009-4025.

Leinfelder, R.R., Nose, M. Schmid, D., Werner, W., 2004. Reefs and carbonate platforms in amixed carbonate-siliciclastic setting. Examples from the UpperJurassic (Kimmeridgian to Tithonian) of west-central Portugal. Pre-Meeting Field Trip A6, 23rd IAS Meeting, Coimbra, 15-17 September.

Liechoscki de Paula Faria, D., dos Reis, A.T., Gomes de Souza, O., 2017. Three-dimensional stratigraphic-sedimentological forward modeling of an Aptian carbonate reservoir deposited during the sag stage in the Santos Basin, Brazil. Marine and Petroleum Geology 88, 676-695.

Lu, P., Cantrell, D., 2016. Reactive transport modelling of reflux dolomitization in the Arab-d reservoir, Ghawar field, Saudi Arabia. Sedimentology 63, 865-892.

Lucia, J.F., 1999. Carbonate Reservoir Characterization. An Integrated Approach - Second Edition. Springer-Verlag, Berlin Heidelberg, 341 p.

Matsuda, F., Saito, M, Iwahashi, R., Oda, H., Tsuji, Y., 2004. Computer Simulation of Carbonate Sedimentary and Shallow Diagenetic Processes. In: Grammer, G.M., Harris, P.M., Eberli, G.P. (Eds.), Integration of outcrop and modern analogs in reservoir modelling. AAPG Memoir 80, 365-382.

Matthew, R. K., Frohlich, C. 1987. Forward modeling of bank-margin carbonate diagenesis. Geology 15, 673-676.

Meyers, W. J. 1991. Calcite cement stratigraphy: an overview. In: Barker, C.E., Kopp, O.C. (Eds.), Luminescence microscopy and spectroscopy: qualitative and quantitative applications, SEPM Short course, 25, 133-148.

Mikes, D., 2011. Reservoir characterisation and upscaling: From core to reservoir. Verlag & Müller, Berlin, 196 p.

Moore, C.H., 2001. Carbonate Reservoirs. Porosity Evolution and Diagenesis in a Sequence Stratigraphic Framework. Developments in Sedimentology 55, Elsevier Science Ldt., Amsterdam, 444 p.

Morse, J.W., Andersson, A.J., Mackenzie, F.T., 2006. Initial responses of carbonate-rich shelf sediments to rising atmospheric pCO2 and ‘‘ocean acidification’’: role of high Mg-calcites. Geochimica Cosmochimica Acta 70, 5814-5830.

Morse, J.W., Mackenzie, F.T., 1990. Geochemistry of Sedimentary Carbonates. New York, Elsevier Scientific Publ. Co., 696 p.

Moutte, J., 2009. Arxim a library for thermodynamic modeling of fluid - rock systems, École des Mines de Saint Étienne Report, 55 p.

Nader, F.H., 2017. Multi-scale Quantitative Diagenesis and Impacts on Heterogeneity of Carbonate Reservoir Rocks. Advances in Oil and Gas Exploration & Production. Springer International Publishing, 146 p.

Nelson, C.S., 1978. Temperate shelf carbonate sediments in the Cenozoic of New Zealand. Sedimentology 25, 737-771.

Nœtinger, B., Artus, V., Zargar, G., 2005. The future of stochastic and upscaling methods in hydrogeology. Hydrogeology Journal 13, 184-201.

Noetinger, B., Zargar, G., 2004. Multiscale Description and Upscaling of Fluid Flow in Subsurface Reservoirs. Oil & Gas Science and Technology 59(2), 119-139.

Nury, D., 1990. L'Oligocène de Provence méridionale : stratigraphie, dynamique sédimentaire, reconstitutions paléogéographiques. PhD Thesis, Provence University, France, 411 p.

Nury, D., Thomassin, B.A., 1994. Paléoenvironnements tropicaux, marins et lagunaires d'un littoral abrité (fonds meubles à bancs coralliens, lagune évaporitique) à l'Oligocène terminal (région d'Aix-Marseille). Géologie Méditerranéenne 21, 95-108.

Oudet, J., 2008. Étude terre-mer de la transition syn-rift/post-rift sur les marges de l'océan Liguro-Provençal : Apports de la modélisation géologique 3D et de la chronostratigraphie intégrée. PhD Thesis, Provence University, France, 288 p.

Oudet, J., Münch, P., Borgomano, J., Quillevere, F., Melinte-Dobrinescu, M.C., Demory, F., Viseur, S., Cornée, J.-J., 2010. Land and sea study of the northeastern golfe du Lion rifted margin: the Oligocene-Miocene of southern Provence (Nerthe area, SE France). Bulletin de la Société Géologique de France 181(6), 591-607.

Pagani, M., Arthur, M.A., Freeman, K.H., 1999. Miocene evolution of atmospheric carbon dioxide. Paleoceanography and Paleoclimatology 14(3), 273-292.

Palandri, J.L., Kharaka, Y.K., 2004. A compilation of rate parameters of water-mineral interaction kinetics for application to geochemical modeling. U.S. Geological Survey, Open File Report OF 2004-1068, 64 p.

Paterson, R.J., Whitaker, F.F., Smart, P.L., Jones, G.D., Oldham, D., 2008. Controls on early diagenetic overprinting in icehouse carbonates: Insights from modelling hydrological zone residence times using CARB3D+. Journal of Sedimentary Research 78(4), 258-281.

Person, M.A., Garven, G., 1992. Hydrologic constraints on petroleum generation within continental rift basins: Theory and application to the Rhine Graben. AAPG Bulletin 76 (4), 468-488.

Planteblat, C., 2013. Modélisation par automate cellulaire des phénomènes diagénétiques de plateformes carbonatées. Calibration et paramétrage à partir de deux cas d'études : l'Urgonien du Vercors (Crétacé Inférieur, SE France) et les Calcaires Gris du Mont Compomolon (Lias, NE Italie). PhD thesis, Grenoble & Lausanne University, 424 p.

Planteblat, C., G. Massonnat, A. Virgone, B. Caline, and C. Pabian-Goyheneche, 2012. Innovative modelling method of diagenetic overprints in carbonate reservoirs: Abu Dhabi International Petroleum Conference and Exhibition, SPE, Extended Abstracts, SPE-161371, 12 p.

Plummer, L.N., Mackenzie, F.T., 1974. Predicting mineral solubility from rate data: application to the dissolution of magnesian calcites. American Journal of Science 274, 61-83.

Qi, D., Pei, B., 2008. Theory and Methodology for Reservoir Upscaling. Xinjiang Petroleum Geology 29(1), 91-93.

Read, J.F., Osleger, D., Elrick, M., 1991. Two-dimensional modelling of carbonate ramp sequences and component cycles. Kansas Geological Survey Bulletin 233, 473-488.

Renard, P., de Marsily, G., 1997. Calculating equivalent permeability: a review. Adv. Water Resour. 20(5-6), 253-378.

Rezaei, M., Sanz, E., Raeisi, E., Ayora, C., Vázquez-Suñé, E., Carrera, J., 2005. Reactive transport modeling of calcite dissolution in the fresh-salt water mixing zone. Journal of Hydrology 311(1-4), 282-298.

Ricken, W. 1987. The carbonate compaction law: a new tool. Sedimentology 34, 571-584.

Sacchi, Q., Borello, E.S., Weltje, G.J., Dalman, R., 2006. Increasing the predictive power of geostatistical reservoir models by integration of geological constraints from stratigraphic forward modelling. Marine and Petroleum Geology 69, 112-126.

Salas, J., Taberner, C., Esteban, M., Ayora, C., 2007. Hydrothermal dolomitization, mixing corrosion and deep burial porosity formation: numerical results from 1-D reactive transport models, Geofluids 7(2), 99-111.

Santerre, Y., 2010. Influence de la diagenèse précoce sur la dynamique sédimentaire et sur la distribution des propriétés pétrophysiques dans les réservoirs carbonatés. PhD Thesis, Provence University, France, 269 p.

Seard, C., Borgomano, J., Granjeon, D., Camoin, G., 2013. Impact of environmental parameters on coral reef development and drowning: Forward modelling of the last deglacial reefs from Tahiti (French Polynesia; IODP Expedition #310). Sedimentology 60, 1357-1388.

Seranne, M., Benedicto, A., Labaume, P., Truffert, C., Pascal, G., 1995. Structural style and evolution of the Gulf of Lion Oligo-Miocene rifting: role of the Pyrenean orogeny. Marine and Petroleum Geology 12(8), 809-820.

Schlager, W., 2000. Sedimentation rates and growth potential of tropical, cool-water and mud-mound carbonate systems. In: Insalaco, E., Skelton, P.W., Palmer, T.J. (Eds), Carbonate Platform Systems: components and interactions, Geological Society, London, Special Publications, 178, 217-227.

Schlager, W., 2003. Benthic carbonate factories of the Phanerozoic. International Journal of Earth Sciences 92, 445-464.

Simone, L., Carannante, G., 1988. The fate of foramol ("temperate-type") carbonate platforms. Sedimentary Geology 60, 347-354.

Smith, A.M., Nelson, C.S., 2003. Effects of early sea-floor processes on the taphonomy of temperate shelf skeletal carbonate deposits. Earth-Science Reviews 63, 1-31.

Stanienda-Pilecki, K.J., 2018. Magnesium calcite in Muschelkalk limestones of the Polish part of the Germanic Basin. Carbonates and Evaporites 33, 801-821.

Steefel, C.I., MacQuarrie, K.T.B., 1996. Approaches to modeling reactive transport in porous media. Reactive Transport in Porous Media. Rev. Mineral. 34, 83-125.

Trenty, L., Michel, A., Tillier, E., Le Gallo, Y., 2006. A sequential splitting strategy for CO2 storage modeling. ECMOR X-10th European Conference on the Mathematics of Oil Recovery, European Association of Geoscientists & Engineers.

Vacher, H.L., Bengtsson, T.O., Plummer, L.N., 1990. Hydrology of meteoric diagenesis: residence time of meteoric ground water in island fresh-water lenses with application to aragonite-calcite stabilization rate in Bermuda. Geological Society of America Bulletin, 102, 223-232.

Wagner, P.D., Tasker, D.R., Wahlman, G.P., 1995. Reservoir degradation and compartmentalization below subaerial unconformities: limestone examples from West Texas, China, and Oman. In: Budd, D.A., Saller, A.H., Harris, P.M. (Eds.), Unconformities and porosity in carbonate strata, AAPG Memoir 63, 239-258.

Walter, L.M., Morse, J.W., 1984. Magnesian calcite stabilities: A reevaluation. Geochimica Cosmochimica Acta 48, 1059-1069.

Wendte, J., Muir, I., 1995. Recognition and significance of an intraformational unconformity in Late Devonian Swan Hills Reef Complexes, Alberta. In: Budd, D.A., Saller, A.H., Harris, P.M. (Eds.), Unconformities and porosity in carbonate strata, AAPG Memoir 63, 259-278.

Whitaker, F.F., Smart, P., Hague, Y., Waltham, D., Bosence, D., 1999. Structure and function of a coupled two-dimensional diagenetic and sedimentological model of carbonate platform evolution. In: Harbaugh J. W., Watney W. L., Rankey E. C., Slingerland R., Goldstein R. H., Franseen E. K. (Eds.), Numerical Experiments in Stratigraphy: Recent Advances in Stratigraphic and Sedimentologic Computer Simulations, SEPM Special Publication 62, 337-355.

Whitaker, F., Smart, P. L., Jones, G. D., 2004. Dolomitization: from conceptual to numerical models, in The Geometry and Petrogenesis of Dolomite Hydrocarbon Reservoirs. Geological Society, London, Special Publication, 235, 99-139.

Whitaker, F.F., Xiao, Y., 2010. Reactive transport modeling of early burial dolomitization of carbonate platforms by geothermal convection. AAPG Bulletin 94, 889-917.

White, A.F., Peterson, M.L., 1990. Role of the reactive surface area. Characterization in geochemical kinetic models. Chemical modeling of aqueous systems II. American Chemical Society, Washington, 461-475.

Williams, H.D., Burgess, P.M., Wright, V.P., Della Porta, G., Granjeon, D. 2010. Investigating Carbonate Platform Types. Multiple Controls and a Continuum of Geometries. Journal of Sedimentary Research 81 (1), 18-37.

Xiao, Y., Jones, D. (2006) Reactive Transport Modeling of Carbonate and Siliciclastic Diagenesis and Reservoir Quality Prediction. SPE paper #101669.

Yapparova, A., Gabellone, T., Whitaker, F., Kulik, D.A., Matthäi, S.K., 2017. Reactive Transport Modelling of DolomitisationDolomitisation Using the New CSMP++GEM Coupled Code: Governing Equations, Solution Method and Benchmarking Results. Transport in Porous Media 117, 385-413.

Yin, X, Huang, W., Wang, P., Wang, J.,Wang, Q., Yan, D., Zhou, X., 2015. Sedimentary evolution of overlapped sand bodies in terrestrial faulted lacustrine basin. Insights from 3D stratigraphic forward modeling. Marine and Petroleum Geology 86, 1431-1443.

Yose, L.A., Ruf, A.S., Strohmenger, C.J., Schuelke, J.S., Gombos, A., Al-Hosani, I., Al-Maskary, S., Bloch, G., Al-Mehairi, Y., Johnson, I.G., 2006. Three-dimensional characterization of a heterogeneous carbonate reservoir, Lower Cretaceous, Abu Dhabi (United Arab Emirates). In: Harris P.M., Weber, L.J., eds., Giant hydrocarbon reservoirs of the world: From rocks to reservoir characterization and modelling. AAPG Memoir 88, SEPM Special Publication, 173-212.

Zhao, M., Planavsky, N.J., Wei, G., Gong, Z., 2017. Simulating meteoric and mixing-zone diagenesis of marine carbonates via a two-dimensional reactive transport model. GSA Annual Meeting, Seattle, Washington, USA, 22-25 October.

10. Figure captions

Figure 1: A) Geological map of Carry-le-Rouet area, showing the repartition of the different lithostratigraphic units (modified from Andreieff et al., 1972), the sedimentary sections and seismic lines used for the geological characterization (Oudet et al., 2010) and the Dionisos^{Flow} modeling. B) Paleogeographic map of the Liguro-Provencal Basin area, during the rifting period (Late Oligocene to Aquitanian). The proximal sub-basins are progressively invaded by the sea, coming from the South (From Oudet, 2008). Red rectangle corresponds to Fig. 1A. Blue rectangle is the area modeled in Dionisos^{Flow}. A.B.: Arlesien Basin; M.B.: Marseille Basin; V.B.: Villeneuve Basin; G.F.B.: Grand Faraman Basin; N.M.: Nerthe Massif. C) Late Oligocene-Early Miocene sedimentary succession of Carry-le-Rouet, with sequence stratigraphy framework and estimated ages of each sequence boundary (biostratigraphy and magnetostratigraphy; Oudet et al., 2010). The colour code refer to Table 1.

Figure 2: Conceptual depositional model for the Oligo-Aquitanian series in the Carry-le-Rouet area, and distribution of the main facies. Not to scale. The colour code refer to Table 1.

Figure 3: Restored initial substratum position for the modeled area, compared to the paleogeographic map of the Liguro-Provencal Basin area. Grey triangles correspond to the different siliciclastic sources, modeled in Dionisos^{Flow}.

Figure 4: Best-fit Dionisos^{Flow} model, showing the facies distribution at different time steps of the model. The black arrow corresponds to the location of the Carry-Le-Rouet section used as a reference section for the model validation (Fig. 1C and Fig. 8A). The colour code refer to Table 1.

Figure 5: A) Grid used for Coores^{Flow}-Arxim simulations, built from a 2D-section of the Dionisos^{Flow} model. A rough representation of the hydrologic zonation is also represented. The colour code refer to the facies, mineralogical and petrophysical conditions (Table 1) used as the initial conditions of the reactive transport model. The black arrow corresponds to the location of the Carry-Le-Rouet section used as a reference section for the model validation. B) Boundary conditions used in the Coores^{Flow}-Arxim model. The eastern groundwater flow rate is set to nil.

Figure 6: A) and B) Initial aragonite volume fraction in the model (A) and after 27 ky (B). C) and D) Initial HMC volume fraction in the model (C) and after 27 ky (D). E) LMC cement volume fraction in the model after 27 ky. F) Porosity variation in the model after 27 ky.

Figure 7: Mineralogical evolution vs. time for two representative facies: “coral carpets” (F8) and “shallow quartz-rich bioclastic Wst.-Pst.” (F4), in different position of the meteoric and marine phreatic zones.

Figure 8: Main petrographic and petrophysical features of the Carry-Le-Rouet succession (from Hamon et al., 2013 modified) used to validate qualitatively the RTM results. A) Vertical distribution of leached, inverted or preserved mineralogically-unstable allochems and microsparitization of the matrix. B to E) Plane-polarized light (PPL) photomicrographs of representative samples taken just

below the exposure surface, affected by an intense meteoric diagenesis (B and C) or away from the meteoric zone, with remaining marine affinity (C and D). F) Values of initial depositional porosity and final values after diagenesis effect (RTM calculation). C.= LMC cement in a moldic pore (dissolved coral) growing on a crystal silt (C.S.) that suggest dissolution; Φm= Moldic porosity; Fo.= Preserved foraminifers (HMC or aragonite).

Table 2: Facies description and interpretation used for the Dionisos^{Flow} simulations, and corresponding quantitative mineralogy and depositional porosity used for the Coores^{Flow}-Arxim simulations.

Table 2: List of the parameters and boundary conditions used in Dionisos^{Flow} and Coores^{Flow}-Arxim simulations.

Table 3: Elementary compositions of the solutions used in the reactive transport simulations. Modified seawater corresponds to the solution initially saturating the porosity, and rainwater to the solution invading the model through recharge.

Table 4: Thermodynamic and kinetic parameters for the minerals considered in Coores^{Flow}-Arxim simulations.

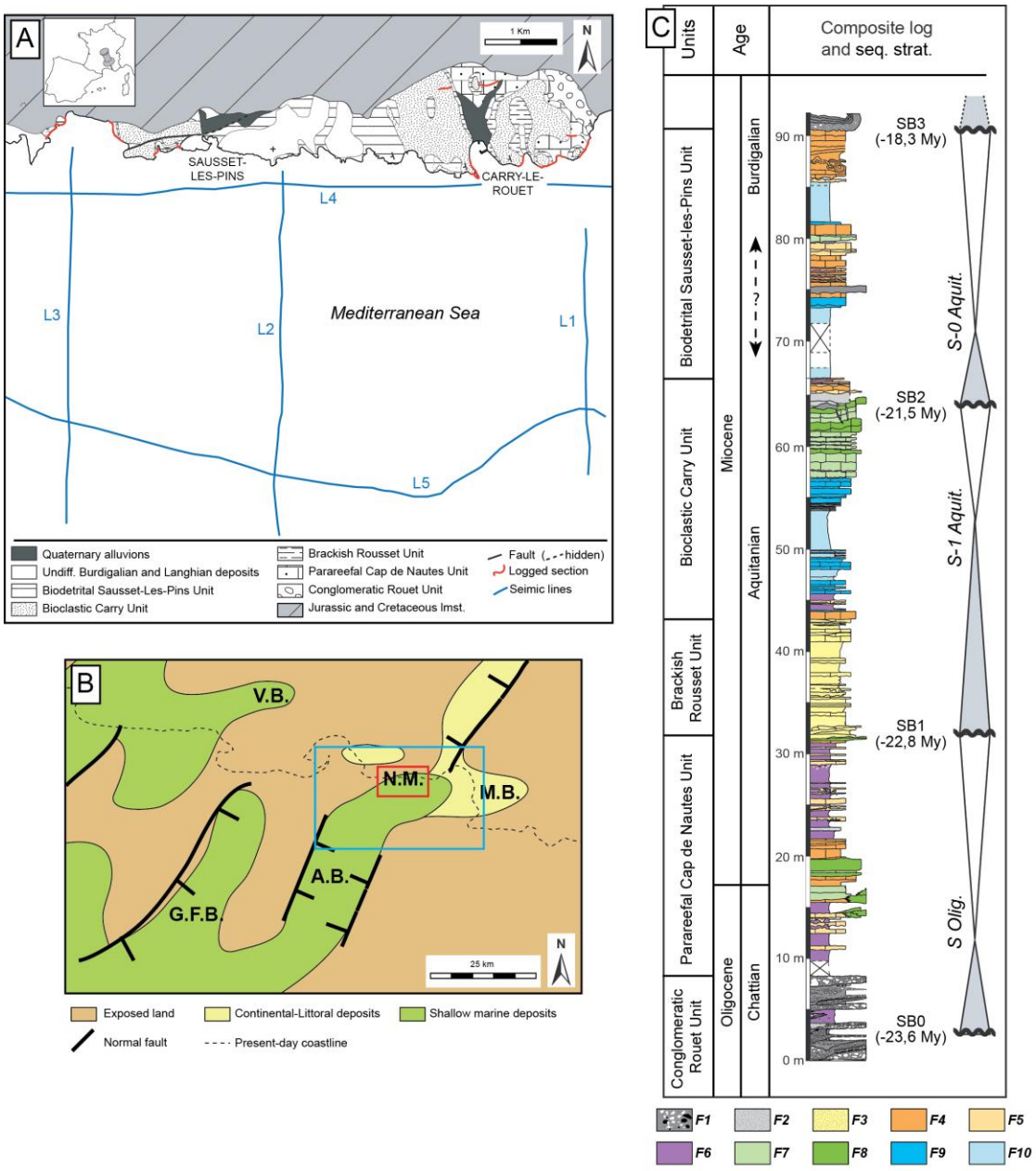
A
1 Km
N
SAUSSET-LES-PINS
CARRY-LE-ROUET
L1
L2
L3
L4
L5
Mediterranean Sea
Quaternary alluvions
Undiff. Burdigalian and Langhian deposits
Biodetrital Sausset-Les-Pins Unit
Bioclastic Carry Unit
Brackish Rousset Unit
Parareefal Cap de Nautes Unit
Conglomeratic Rouet Unit
Jurassic and Cretaceous lmst.
Fault (hidden)
Logged section
Seimic lines
B
V.B.
N.M.
M.B.
A.B.
G.F.B.
25 km
N
Exposed land
Continental-Littoral deposits
Shallow marine deposits
Normal fault
Present-day coastline
C
Units
Age
Composite log and seq. strat.
Biodetrital Sausset-les-Pins Unit
Bioclastic Carry Unit
Brackish Rousset Unit
Parareefal Cap de Nautes Unit
Conglomeratic Rouet Unit
Miocene
Oligocene
Burdigalian
Aquitanian
Chattian
90 m
80 m
70 m
60 m
50 m
40 m
30 m
20 m
10 m
0 m
SB3 (-18,3 My)
SB2 (-21,5 My)
SB1 (-22,8 My)
SB0 (-23,6 My)
S-0 Aquit.
S-1 Aquit.
S Olig.
F1
F2
F3
F4
F5
F6
F7
F8
F9
F10

Figure 1

5

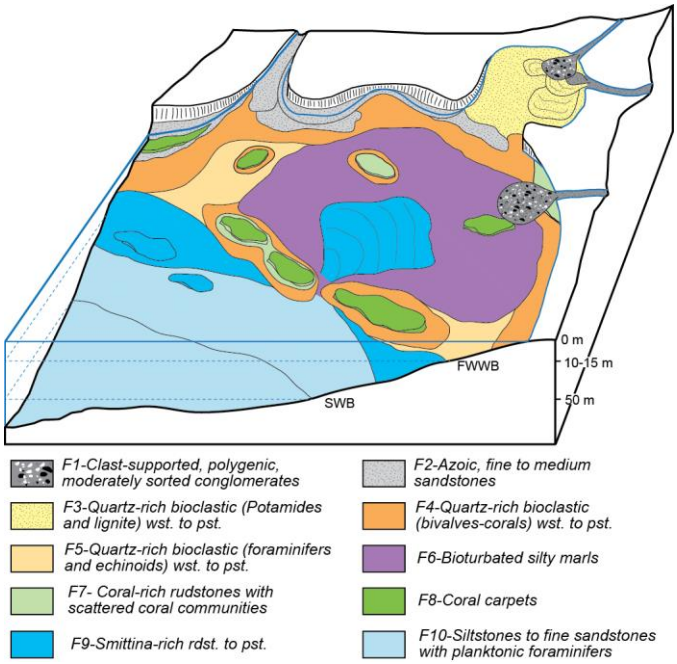
0 m
10-15 m
50 m
FWWB
SWB
F1-Clast-supported, polygenic, moderately sorted conglomerates
F2-Azoic, fine to medium sandstones
F3-Quartz-rich bioclastic (Potamides and lignite) wst. to pst.
F4-Quartz-rich bioclastic (bivalves-corals) wst. to pst.
F5-Quartz-rich bioclastic (foraminifers and echinoids) wst. to pst.
F6-Bioturbated silty marls
F7- Coral-rich rudstones with scattered coral communities
F8-Coral carpets
F9-Smittina-rich rdst. to pst.
F10-Siltstones to fine sandstones with planktonic foraminifers

Figure 2

5

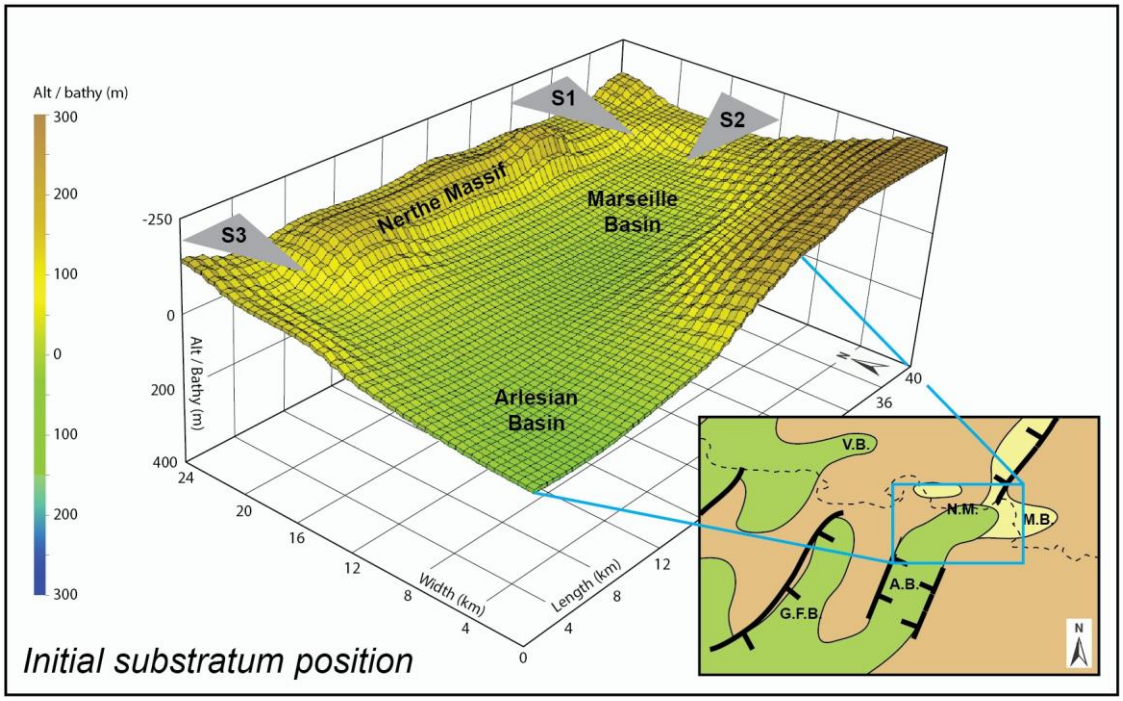
Alt / bathy (m)
300
200
100
0
100
200
300
S1
S2
S3
Nerthe Massif
Marseille Basin
Arlesian Basin
-250
0
200
400
Alt / Bathy (m)
24
20
16
12
8
4
0
Width (km)
Length (km)
12
8
4
0
36
40
V.B.
N.M.
M.B.
A.B.
G.F.B.
N
Initial substratum position

Figure 3

5

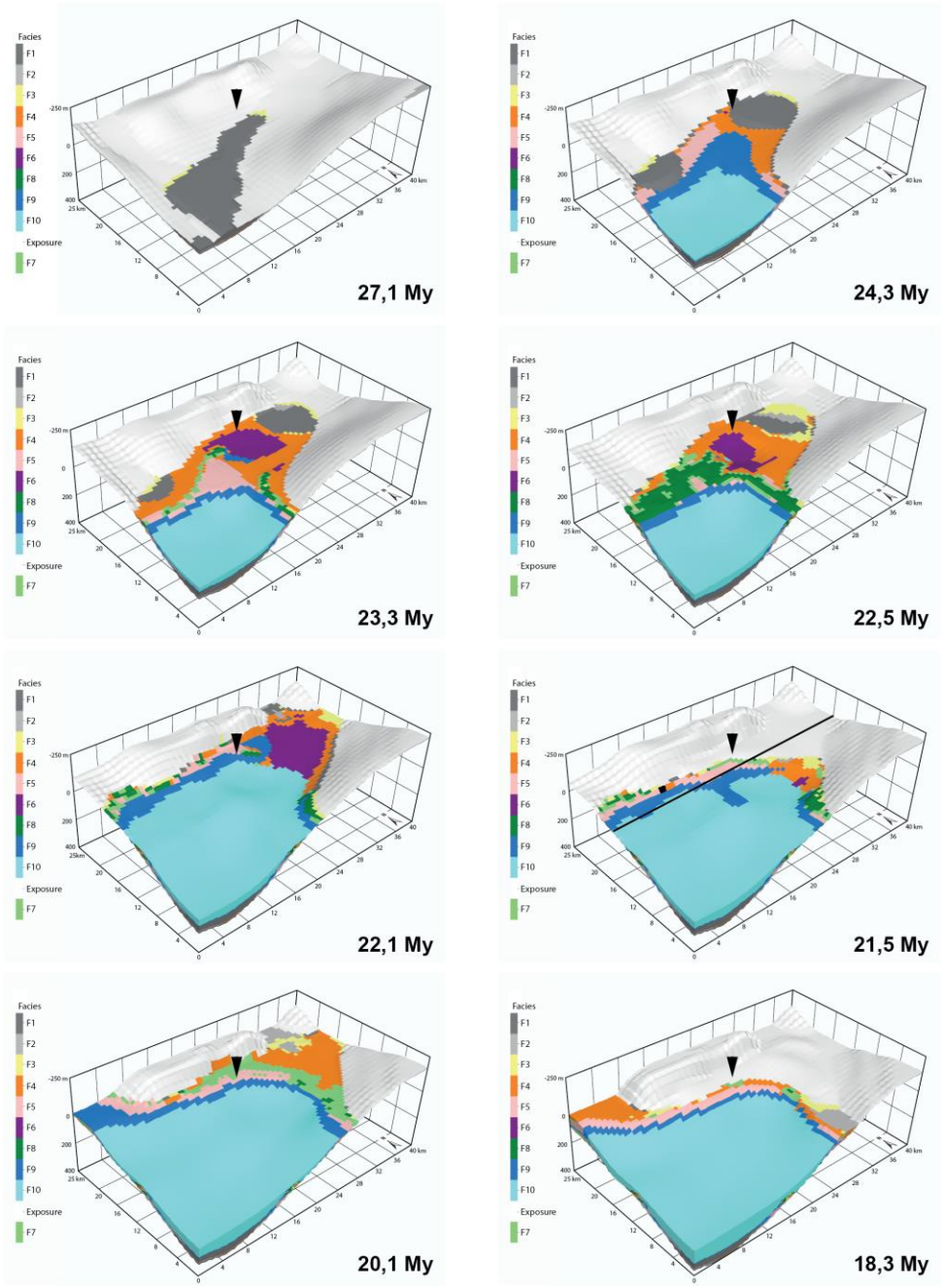
Facies
F1
F2
F3
F4
F5
F6
F8
F9
F10
Exposure
F7
27,1 My
24,3 My
23,3 My
22,5 My
22,1 My
21,5 My
20,1 My
18,3 My

Figure 4

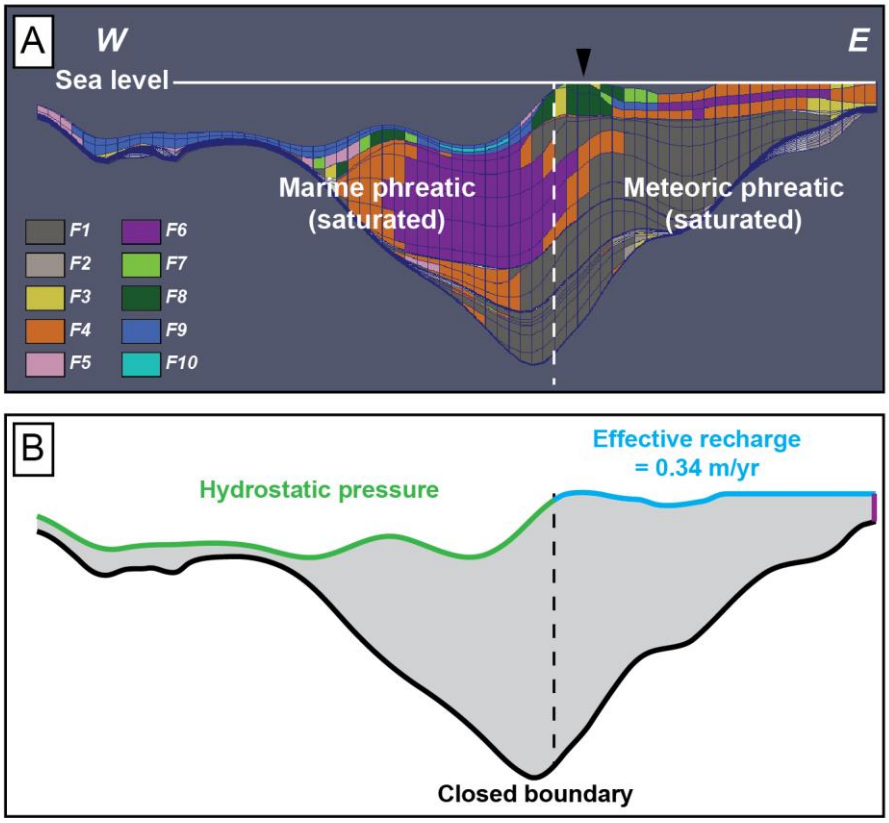
A
W
E
Sea level
Marine phreatic
(saturated)
Meteoric phreatic
(saturated)
F1
F2
F3
F4
F5
F6
F7
F8
F9
F10
B
Effective recharge
= 0.34 m/yr
Hydrostatic pressure
Closed boundary

Figure 5

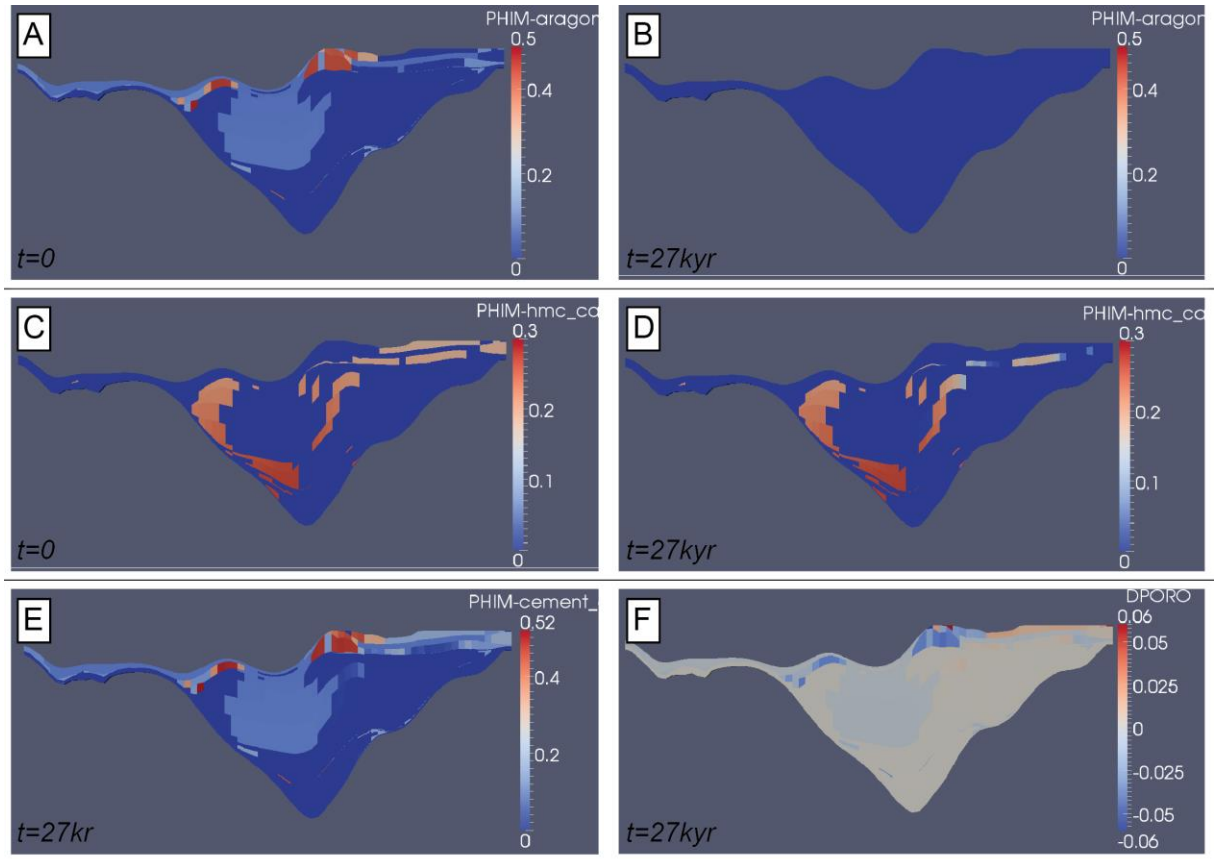
A
PHIM-aragor
0.5
0.4
0.2
0
t=0
B
PHIM-aragor
0.5
0.4
0.2
0
t=27kyr
C
PHIM-hmc_ca
0.3
0.2
0.1
0
t=0
D
PHIM-hmc_ca
0.3
0.2
0.1
0
t=27kyr
E
PHIM-cement_
0.52
0.4
0.2
0
t=27kr
F
DPORO
0.06
0.05
0.025
0
-0.025
-0.05
-0.06
t=27kyr

Figure 6

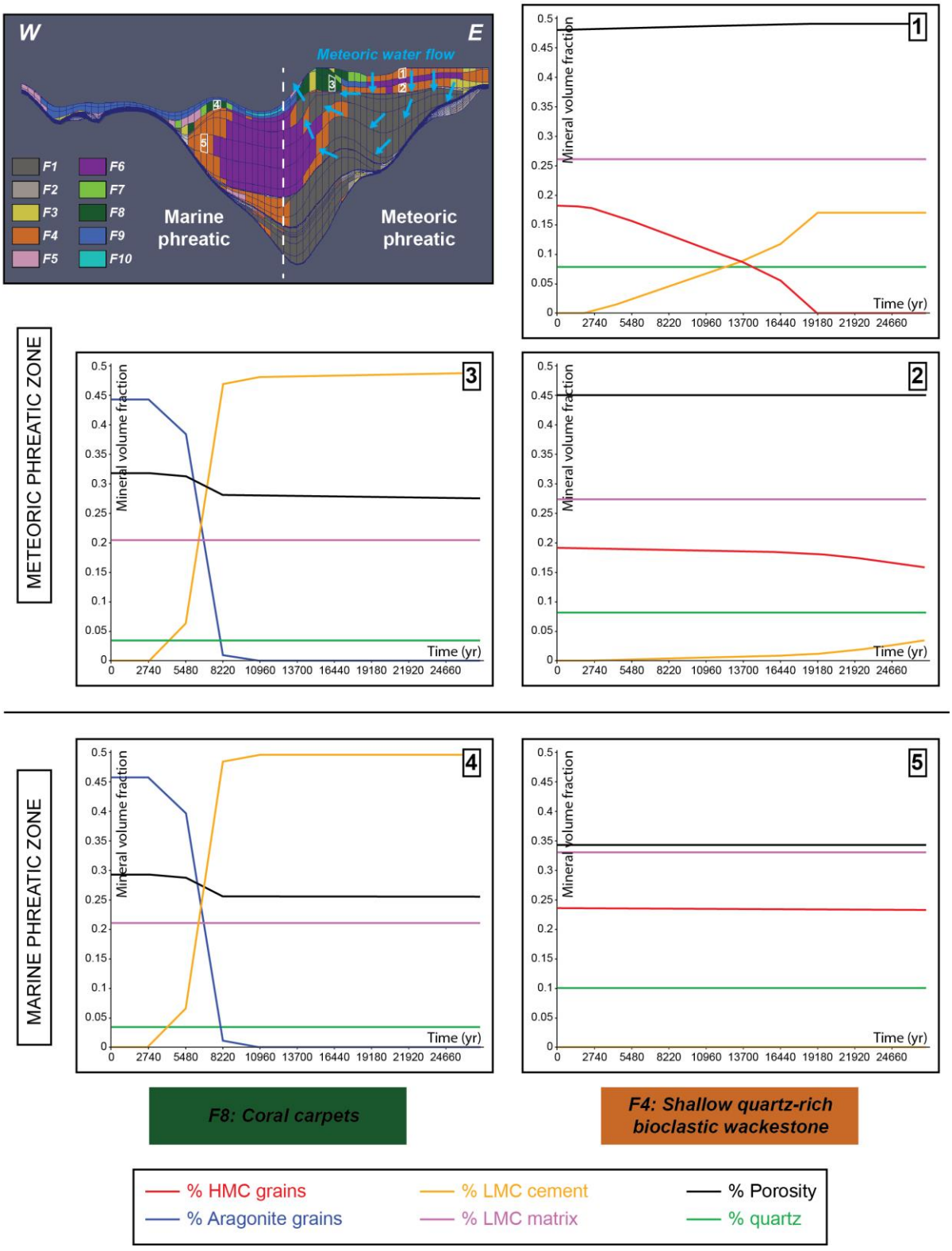
W
E
Meteoric water flow
F1
F2
F3
F4
F5
F6
F7
F8
F9
F10
Marine phreatic
Meteoric phreatic
METEORIC PHREATIC ZONE
MARINE PHREATIC ZONE
Mineral volume fraction
Time (yr)
0 2740 5480 8220 10960 13700 16440 19180 21920 24660
1
2
3
4
5
F8: Coral carpets
F4: Shallow quartz-rich bioclastic wackestone
% HMC grains
% Aragonite grains
% LMC cement
% LMC matrix
% Porosity
% quartz

Figure 7

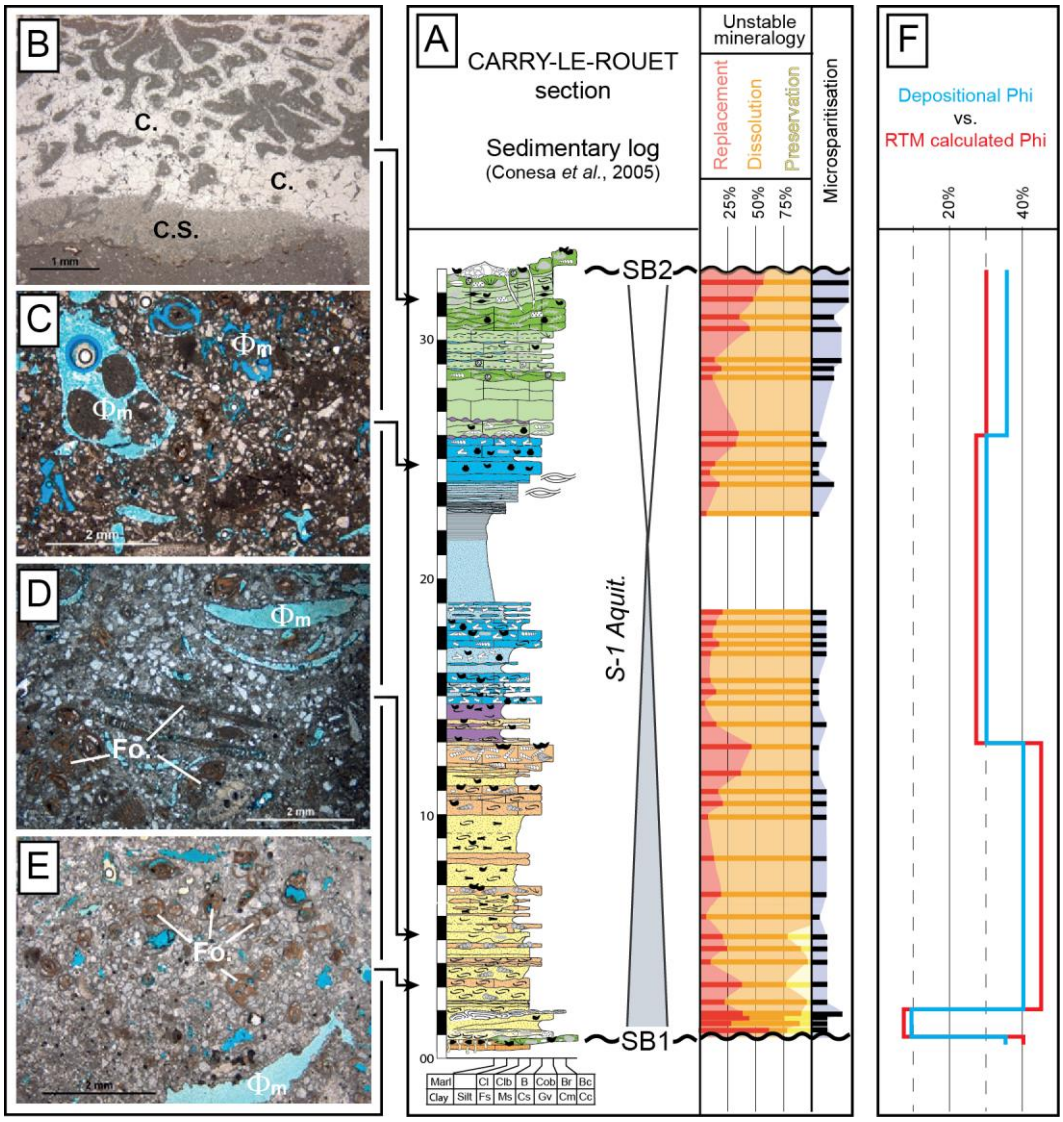
B
C.
C.
C.S.
1 mm
C
Φm
Φm
2 mm
D
Φm
Fo.
2 mm
E
Fo.
2 mm
Φm
A
CARRY-LE-ROUET
section
Sedimentary log
(Conesa et al., 2005)
Unstable
mineralogy
Replacement
Dissolution
Preservation
Microsparitisation
25%
50%
75%
SB2
SB1
S-1 Aquit.
30
20
10
00
Marl
Clay
Silt
Cl
Fs
Clb
Ms
B
Cs
Cob
Gv
Br
Cm
Bc
Cc
F
Depositional Phi
vs.
RTM calculated Phi
20%
40%

Figure 8

	Facies	Lithology	Components	Interpretation	Quantitative mineralogy	Depositional porosity
F1	Clast-supported, polygenic, moderately sorted conglomerates	- Clast supported, polygenic, moderately sorted conglomerates - Sheet morphology, channelized bedforms	- Rounded, Urgonian limestone clasts, granule to cobble in size - Quartz-rich bioclastic matrix (Ostreidae, gastropods, miliolids, Microcodium)	Sheetfloods at the mouth of a gravely river accumulated and reworked in a shallow, coastal setting	- Quartz: 10% - Grains (pluri-cm; 60%): LMC - Matrix (30%): LMC	Φ dep: 10 %
F2	Azoic, fine to medium sandstones	- Well-sorted, fine to medium sandstones - Wave ripples - Thalassinoides and Ophiomorpha burrows	- Rare unidentified bioclasts and Microcodium debris - Subangular quartz and feldspars, 50 to 250 µm - Urgonian micritic lithoclasts	Moderate to high-energy shoreface, closed to fluvial mouth	- Quartz: 80% - Grains (mm; 20%): LMC	Φ dep: 35 %
F3	Quartz-rich bioclastic (Potamides and lignite) wackestones to packstones	- Quartz-rich bioclastic wst. to pst., wave ripples	- Potamides and Neretidae - Ostreidae, other bivalves, stromatolite clasts - Poorly-sorted quartz grains (50 to 500 µm) - Millimetric clasts of lignite	Low-energy, anoxic to dysoxic shallow environment-Brackish conditions	- Quartz: 30% - Grains (mm; 20%): aragonite - Matrix (50%): LMC	Φ dep: 40 %
F4	Quartz-rich bioclastic (bivalves-corals) wackestones-packstones	- Quartz-rich bioclastic wst. to pst., wave ripples - Thalassinoides bioturbations	- Bioclasts of bivalves, benthic foram., Corallinaceae, coral debris, rare Cirripedia - Peloids, subangulous quartz grains (50-250 µm)	- Moderate-energy, stenohaline, infralittoral environments - Shallow inner-shelf setting	- Quartz: 10% - Grains (mm; 30%): HMC - Grains (mm ; 10%): aragonite - Matrix (50%): LMC	Φ dep: 40 %
F5	Quartz-rich bioclastic (foraminifers-echinoids) wackestones-packstones	- Quartz-rich bioclastic wst. to pst. - Badly expressed wave ripples	- Miliolidae, Austrotrillinidae, Amphisteginidae, Lepidocyclinidae, Myogypsinidae - Bioclasts of bivalve, echinoids, and red algae (Corallinaceae)	Low-energy, marine setting emplaced in a deeper inner-shelf to mid-shelf	- Quartz: 10% - Grains (mm; 20%): HMC - Grains (mm; 15%): aragonite - Grains (mm; 5%): LMC - Matrix (50%): LMC	Φ dep: 40 %
F6	Bioturbated silty marls	- Dark, greyish silty marls - Thalassinoides burrows	- Local lumachellic lags (bivalves) - Millimetric to centimetric clasts of lignite	Low-energy badly oxygenated deeper inner-shelf	- Quartz: 40% - Grains (mm; 10%): aragonite - Matrix (50%): LMC	Φ dep: 30 %
F7	Coral-rich rudstones with scattered coral communities	- Coral bafflestones, coral-rich rudstones - Patchy, non-framework communities	- Corals: Porites, Tarbellastraea, Caulastraea, Mussimilia - Acropora debris, red algae, serpulids, Ostreidae, rare echinoids, Lepidocyclinidae	Non-framebuilding coral communities, passing laterally into one another or into coral-rich rudstones (reworking breccia)	- Quartz: 10% - Grains (mm; 50%): aragonite - Matrix (40%): LMC	Φ dep : 30 %

F8	Coral carpets	- Coral framestones–bafflestones - Flat layers of low topographic relief, 500 m of lateral extent	- Corals (s.l.): Porites, Tarbellastraea, Millepora… - Red algae, serpulids, Ostreidae, rare echinoids	Isolated frame-building coral carpets (maximum two to three generations) in inner-shelf setting	- Quartz: 5% - Carbonate grains - mm; aragonite : 65% - Matrix (30%): LMC	Φ dep : 35 %
F9	Smittina-rich rudstones to packstones	- Quartz-rich bioclastic rst. to pst. - Flat layers of low topographic relief, 300 m of lateral extent	- Monogeneric bryozoan debris (Smittina) - Coral debris (Porites, Caulastraea), echinoderms (Scutella), Ostreidae, Pectinidae, Gastropods, red algae debris	Reworking and mixing of Smittina colonies formed in lower infralittoral to upper circalittoral environment	- Quartz: 10% - Carbonate grains - mm; aragonite : 10% - Carbonate grains - mm; LMC : 50% - Matrix (30%): LMC	Φ dep : 30 %
F10	Siltst. to fine sandstones with planktonic foraminifers	- Yellowish, unconsolidated, well- sorted, siltstones to fine sandstones - Planar lamination, episodic HCS - Heavily bioturbated (Thalassinoides)	- Globigerinidae, silty quartz, glauconite grains	Low-energy, open-marine, offshore, and relatively deep conditions with episodic storm events	- Quartz: 40% - Carbonate grains - mm; LMC : 10% - Matrix (50%): LMC	Φ dep : 30 %

Table 3

Parameters	Values
Dionisos^{Flow}	
Model type and size	3D block - 40x25 km^2
Cell dimension	500x500 m
Display time	9.8 My
Time step	100 ky
Subsidence	15 m/Ma (Unit 3) to 80 m/Ma (Unit 2).
Minimum wave energy threshold	10 to 40 $kW.m^{-1}$
Wave action depth	20 m with a maximum of energy at 10 m
Wave propagation angle	Az : 30°
Maximum production rate	0.01 to 0.7 mm/yr
External sediment supply	S1: 0.25 to 1,64 km^3/My S2: 0 to 0,75 km^3/My S3: 0,25 to 2 km^3/My
Total Fluvial discharge	200 to 700 m^3/s
Erosion	0
Water-driven transport K (diffusion coefficient)	0 to 0,01 km^2/ky
Coores-Arxim	
Model type and size	Vertical 2D-section 36.5 km long x 500 m (1 cell) wide x 4 to 132 m high
Cell dimension	500x500 m
Display time	27 ky (9.9×10^6days)
Time step	1 day
Meteoric recharge	0.34 m/yr (1200 mm mean annual precipitation)
Groundwater recharge	Flow rate of 0 m/y at the eastern boundary

Table 2

pH and elementary concentrations (in mol/kgH_2O)	pH at 25°C	C	Ca	Cl	K	Mg	Na	S	Si
Modified seawater	7.56	2.1×10^{-3}	9.8×10^{-3}	5.472×10^{-1}	1×10^{-4}	5.29×10^{-2}	4.700×10^{-1}	2.83×10^{-2}	1×10^{-4}
Rainwater	6.63	1.0×10^{-3}	2×10^{-4}	1×10^{-6}	1×10^{-6}	1×10^{-6}	1×10^{-6}	1×10^{-6}	1×10^{-6}

Table 3

Reactive mineral	Formula	logK @ 25°C	Dissolution kinetic constant (mol/m²/s)	Precipitation kinetic constant (mol/m²/s)	Initial grain radius (m)
Aragonite	$CaCO_3$	8.34	$10^{-9.46}$	$10^{-9.46}$	10^{-4}
Mg-rich Calcite (HMC)	$Ca_{0.88}Mg_{0.12}CO_3$	8.34	$10^{-5.51}$	$10^{-9.76}$	10^{-4}
Low-Mg calcite (cement calcite)	$CaCO_3$	8.48	$10^{-9.46}$	$10^{-9.46}$	10^{-4}
Quartz	SiO_2	4.00	$10^{-13.4}$	$10^{-13.4}$	10^{-4}

Table 4